

## **CdSe@CdS Dot@Platelet Nanocrystals: Controlled Epitaxy, Mono-Exponential Decay of Two-Dimensional Exciton, and Non-Blinking Photoluminescence of Single Nanocrystal**

Yonghong Wang, Chaodan Pu, Hairui Lei, Haiyan Qin, and Xiaogang Peng

*J. Am. Chem. Soc.*, **Just Accepted Manuscript** • DOI: 10.1021/jacs.9b06932 • Publication Date (Web): 14 Oct 2019

Downloaded from [pubs.acs.org](https://pubs.acs.org) on October 15, 2019

### **Just Accepted**

“Just Accepted” manuscripts have been peer-reviewed and accepted for publication. They are posted online prior to technical editing, formatting for publication and author proofing. The American Chemical Society provides “Just Accepted” as a service to the research community to expedite the dissemination of scientific material as soon as possible after acceptance. “Just Accepted” manuscripts appear in full in PDF format accompanied by an HTML abstract. “Just Accepted” manuscripts have been fully peer reviewed, but should not be considered the official version of record. They are citable by the Digital Object Identifier (DOI®). “Just Accepted” is an optional service offered to authors. Therefore, the “Just Accepted” Web site may not include all articles that will be published in the journal. After a manuscript is technically edited and formatted, it will be removed from the “Just Accepted” Web site and published as an ASAP article. Note that technical editing may introduce minor changes to the manuscript text and/or graphics which could affect content, and all legal disclaimers and ethical guidelines that apply to the journal pertain. ACS cannot be held responsible for errors or consequences arising from the use of information contained in these “Just Accepted” manuscripts.

1  
2  
3  
4 **CdSe@CdS Dot@Platelet Nanocrystals: Controlled Epitaxy, Mono-Exponential Decay of Two-**  
5  
6 **Dimensional Exciton, and Non-Blinking Photoluminescence of Single Nanocrystal**  
7

8 Yonghong Wang†, Chaodan Pu†, Hairui Lei, Haiyan Qin, Xiaogang Peng\*

9  
10 *Center for Chemistry of Novel & High-Performance Materials, Department of Chemistry, Zhejiang*

11  
12  
13 *University, Hangzhou 310027, China.*  
14  
15  
16

17 **ABSTRACT:** *Wurtzite CdSe@CdS dot@platelet nanocrystals—a dot-shaped CdSe nanocrystal encased within an*  
18 *epitaxially-grown CdS nanoplatelet—are controllably synthesized with nearly monodisperse size/shape distribution*  
19 *and outstanding photoluminescence (PL) properties. The excellent size/shape control with their lateral to thickness*  
20 *dimension ratio up to 3 to 1 is achieved by systematically studying the synthetic parameters, which results in a simple,*  
21 *tunable yet reproducible epitaxy scheme. This special type of core/shell nanocrystals possess two-dimensional*  
22 *emission dipole with the ab plane of the wurtzite structure. While their near-unity PL quantum yield and mono-*  
23 *exponential PL decay dynamics are at the same level of the-state-of-art CdSe/CdS core/shell nanocrystals in dot*  
24 *shape, CdSe@CdS dot@platelet nanocrystals possess ~2 orders of magnitude lower probability for initiating PL*  
25 *blinking at single-nanocrystal level than the dot-shaped counterparts do.*  
26  
27  
28  
29  
30  
31  
32  
33  
34  
35  
36  
37  
38  
39  
40  
41  
42  
43  
44  
45  
46  
47  
48  
49  
50  
51  
52  
53  
54  
55  
56

## INTRODUCTION

Colloidal semiconductor nanocrystals with all three dimensions smaller than the exciton size (0D nanocrystals) <sup>1</sup> have been playing a visible role in industrial applications as color-tunable, ultra-pure, highly efficient, and stable emissive materials. Semiconductor nanocrystals with two dimensions greater than the exciton size (2D nanocrystals) possess interesting emission properties due to their unique electronic structures. Upon photo- or electro-excitation, the emission transition dipole of a band-edge exciton within a 2D nanocrystal is often found to locate in its lateral plane perpendicular to the thickness direction, resulting in polarized/directional luminescence, <sup>2-5</sup> which are desirable for applications for lighting-emitting-diodes and lasers. 2D nanocrystals of II-VI semiconductors can be synthesized with atomically flat basal planes to yield extremely narrow emission line, <sup>6-9</sup> ideal for display applications. Anisotropic shape of 2D nanocrystals has been reported to act as a tool to reduce degeneracy of the band-edge hole states, <sup>4, 10-13</sup> which is of critical importance for lasers. However, in comparison with luminescence properties of best developed 0D nanocrystals, emission properties of colloidal 2D nanocrystals are far from being ideal. At present, studies on semiconductor nanocrystals are mostly focused on II-VI and III-V ones that are in either wurtzite (hexagonal) or zinc-blende (face-centered cubic) structure. As a result, the corresponding 2D nanocrystals, including the application-relevant core/shell ones, are synthetically challenging and requires specific control of the growth kinetics in a generally non-favorable manner. <sup>9, 14-17</sup> For example, the easy-growth axis of wurtzite nanocrystals is its c-axis, which would thus result in a rod-shaped <sup>18-19</sup> and elongated spheroidal <sup>20-21</sup> nanocrystals, instead of disk-shaped 2D nanocrystals.

Core/shell nanocrystals with a narrow bandgap core and epitaxially-grown wide bandgap shells are regarded as necessary structure for ideal luminescence properties in applications. Though plain core 2D nanocrystals could be synthesized with atomically-flat basal planes for both zinc-blende <sup>7-8, 22-23</sup> and wurtzite <sup>6, 9</sup> structures, their

1  
2  
3 structural integrity and luminescence properties are difficult to maintain during epitaxial growth of wide-  
4 bandgap shells.<sup>24-26</sup> The other class of structure that could realize luminescence properties of 2D nanocrystals  
5  
6 consists of a spheroidal core with narrow bandgap and epitaxially grown disk-shaped shells with wide bandgap,  
7  
8 in which the wavefunctions would be partially extended from the core dot into the platelet shell and result in a  
9  
10 2D system.<sup>10,12,27</sup> Though structure of the second class of 2D nanocrystals is less defined and their luminescence  
11  
12 properties are poor at present, they are presumably flexible in synthesis. Such flexibility is necessary in the  
13  
14 further development of emitters with ideal 2D emission properties. As shown in the case of 0D nanocrystals, it  
15  
16 would be crucial to adjust the surface configuration to eliminate electron/hole traps for nearly unity  
17  
18 photoluminescence (PL) quantum yield (QY), mono-exponential PL decay dynamics, and single-dot non-  
19  
20 blinking PL.<sup>28</sup> PL blinking refers to, for a single-nanocrystal, random switching of its PL intensity under  
21  
22 constant excitation, which was discovered about 20 years ago and has been a significant challenge for colloidal  
23  
24 semiconductor nanocrystals.<sup>29-31</sup> To the best of knowledge, there is no report on nearly non-blinking 2D  
25  
26 nanocrystals at present.<sup>32</sup>

27  
28  
29  
30  
31  
32  
33  
34  
35  
36  
37 Similar to 0D nanocrystals, CdSe and related II-VI semiconductors are mostly studied for 2D nanocrystals.<sup>8-9,</sup>  
38  
39  
40  
41  
42  
43  
44  
45  
46  
47  
48  
49  
50  
51  
52  
53  
54  
55  
56  
57  
58  
59  
60

<sup>16, 33-35</sup> A typical example of the second class of 2D nanocrystals is a wurtzite CdSe dot encased in a CdS  
nanoplatelet (CdSe@CdS dot@platelet) 2D nanocrystals, which was introduced in 2012 by the Durbetret group.  
<sup>10</sup> By annealing the Cd precursor (CdO and oleic acid mixture in octadecene (ODE)) at 300 °C prior to  
introducing the S precursors, they observed formation of CdSe@CdS dot@platelet 2D nanocrystals using a  
conventional Successive-Ion-Layer-Adsorption-and-Reaction (SILAR) protocol developed for synthesizing  
spheroidal CdSe/CdS core/shell nanocrystals. Though size/shape distribution was not well controlled, they  
demonstrated most of interesting properties of the 2D nanocrystals. The Sargent group recently showed that, by

1  
2  
3 increasing the epitaxial temperature to 300-310 °C and applying a mixed ligand system, it would be possible to  
4  
5 switch between lateral and c-axis growth of the wurtzite CdSe/CdS lattice.<sup>12</sup> The Deka group reported that, for  
6  
7 epitaxial growth of wurtzite CdS shells onto CdSe core dots, fatty amines—mixed with other types of ligands—  
8  
9 were critical reagents to induce rapid growth at 335-370 °C along the lateral directions and retard the growth  
10  
11 along the c-axis.<sup>27</sup> Though size/shape distribution of CdSe@CdS dot@platelet 2D nanocrystals in Deka's report  
12  
13 was not ideal, they observed rectangular side view of a significant portion of the nanocrystals.<sup>27</sup>  
14  
15  
16  
17  
18  
19

20  
21 Wurtzite CdSe—the same for wurtzite CdS—is in hexagonal phase with a unique and polar c-axis, which is  
22  
23 different from their zinc-blende (face-centered cubic) counterparts with their a, b, and c axes being equal. Thus,  
24  
25 the thermodynamically preferred shape of wurtzite CdSe and CdS should be hexagons slightly elongated along  
26  
27 the c-axis.<sup>36</sup> Taking the kinetic advantage of the Se-terminated  $[00\bar{1}]$  facet,<sup>37-38</sup> one can synthesize nearly  
28  
29 monodisperse CdSe nano-rods by applying appropriate ligands.<sup>18</sup> Opposite to the growth pattern of wurtzite  
30  
31 CdSe nano-rods, formation of wurtzite CdSe 2D nanocrystals would require a and b axes to become preferential  
32  
33 growth fronts over the c-axis. It should be mentioned that formation of wurtzite CdSe core nanoplatelets was  
34  
35 observed through oriented attachment,<sup>39-40</sup> which is difficult to be realized for the core/shell ones.  
36  
37  
38  
39  
40  
41  
42

43 It is interesting to notice that wurtzite CdSe quasi-2D nanocrystals with a trapezoidal side view and hexagonal  
44  
45 top view were reported by the Stoykovich group using a seeded approach at 370 °C with very high precursor  
46  
47 concentrations.<sup>41</sup> When the reaction temperature was reduced to 345 °C, the same system would no longer  
48  
49 produce the quasi-2D nanocrystals. Though not for synthesizing CdSe@CdS dot@platelet 2D nanocrystals, the  
50  
51 Chen group found that, by adjusting ligand composition, it was possible to synthesize highly faceted pyramid  
52  
53 and bi-pyramid CdSe/CdS core/shell nanocrystals in wurtzite structure.<sup>42</sup>  
54  
55  
56  
57  
58  
59  
60

1  
2  
3  
4  
5  
6 Overall, in the limited examples for growth of wurtzite CdSe and CdSe@CdS dot@platelet 2D nanocrystals,  
7  
8 special ligands, including phosphonic acids, annealed fatty acids, and/or fatty amines, were suggested to play a  
9  
10 decisive role.<sup>10,27</sup> According to our recent work, on-surface chemical reactions for growth of CdSe nanocrystals  
11  
12 would be greatly affected by bonding modes of the surface ligands.<sup>43</sup> When carboxylate and phosphonate  
13  
14 ligands, especially the latter, are tightly bonded onto the nanocrystal surface, it would result in a substantially  
15  
16 high activation energy for the on-surface chemical reactions.<sup>42-43</sup> However, it is unclear what would be an ideal  
17  
18 ligand system to tune the growth modes for 2D nanocrystals. In addition, all ligand systems applied so far for  
19  
20 synthesizing 2D nanocrystals were quite complex and role of each component was barely identified.  
21  
22  
23  
24  
25  
26  
27

28 To achieve kinetic control of the shape, the key is to control the on-surface reactions involved in epitaxial growth  
29  
30 of the CdS shells. For any kinetic-controlled system, in addition to nature of surface ligands, concentration of  
31  
32 surface ligands might also play a key role, which means that it would be desirable to study ligand effects in a  
33  
34 quantitative manner. For binary compound nanocrystals (CdSe and CdS in the current work), reaction kinetics  
35  
36 of epitaxy might be drastically different by switching the position of cationic and anionic species, namely, either  
37  
38 on the nanocrystal surface or in the solution.<sup>43</sup> As for reaction temperature, discussions above suggest that it  
39  
40 should be considered in combination with the ligands. After systematically examining these hypotheses, we aim  
41  
42 to further explore means for synthetically control of the excited states<sup>28</sup> of CdSe@CdS dot@platelet 2D  
43  
44 nanocrystals. The overall efforts result in monodisperse 2D nanocrystals with near-unity PL QY, mono-  
45  
46 exponential PL decay dynamics, polarized PL, and non-blinking PL of single 2D nanocrystal.  
47  
48  
49  
50  
51  
52  
53  
54  
55  
56  
57  
58  
59  
60

## RESULTS AND DISCUSSION

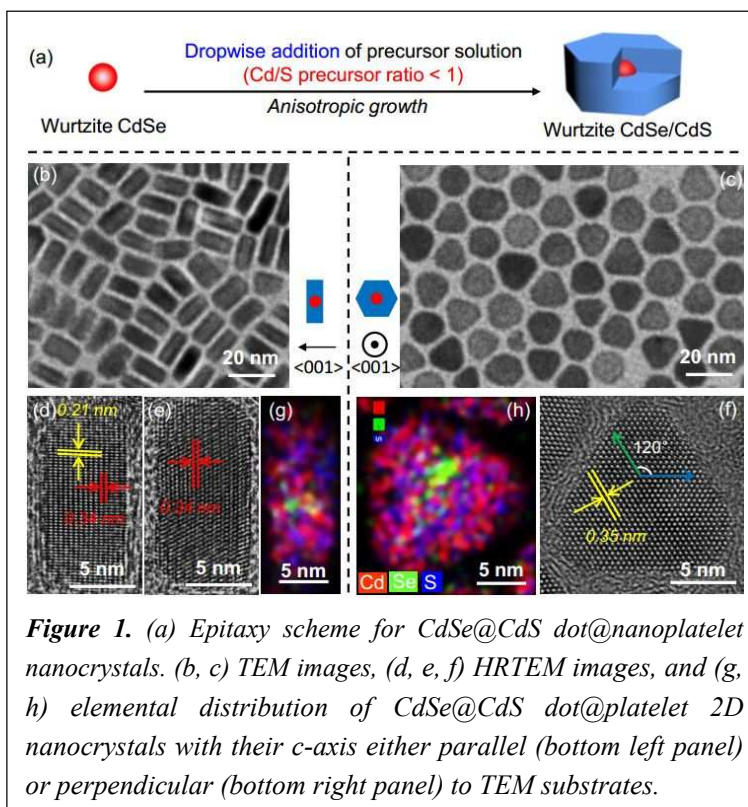
**Choice of synthetic system.** Wurtzite CdSe spheroidal core nanocrystals are synthesized through a well-established “greener approach”, which resulted in spheroidal CdSe/CdS core/shell nanocrystals through the conventional SILAR approach.<sup>21</sup> We intend to develop a new epitaxy scheme to alter the shape of the epitaxial CdS shells to grow CdSe@CdS dot@platelet 2D nanocrystals from these generic CdSe core nanocrystals. The new scheme should be simple for both practical and fundamental reasons. A simple system would make the mass production cost-effective. Fundamentally, a simple epitaxial scheme would make systematic studies relatively easy to carry out.

We decide to exclude phosphonic acids and cadmium phosphonates from the epitaxial growth though they have been widely applied previously for shape-controlled synthesis of CdSe nanocrystals.<sup>18, 27, 41, 44-46</sup> This is so because phosphonate and cadmium phosphonate ligands bonded to surface of nanocrystals very strongly, which would require very high growth temperatures.<sup>18, 41, 47</sup> In literature, high temperatures are identified to eliminate well-defined facets on CdSe nanocrystals, leading to spheroidal shape.<sup>37, 42, 48</sup> We also exclude thiols and tertiary phosphines,<sup>49-51</sup> whose roles in epitaxy can be complicated to be quantified. ODE is chosen as the non-coordinating solvent. Cadmium fatty acid salts (Cd(Fa)<sub>2</sub>) and elemental S are the cationic and anionic precursors, respectively. Fatty amines and fatty acids may be used as additional ligands/additives and will be studied in detail.

Figure 1a illustrates the main differences between the conventional SILAR approach<sup>21</sup> and the current approach for epitaxial growth of the CdS shells onto wurtzite CdSe core, i.e., dropwise addition of a mixed precursor solution with the Cd to S precursor molar ratio being less than one to one (Cd/S < 1).

**Structure identification of CdSe@CdS dot@platelet 2D nanocrystals.** When the concentration of

CdSe@CdS dot@platelet 2D nanocrystals in the solution is sufficiently high for depositing onto the transmission electron microscope (TEM) substrates, they could have their thickness direction either perpendicular or parallel to the electron beam, each of which would usually appear in sizable domains on the substrates. Figures 1b-f illustrate a series of TEM images for one sample with the CdS shells epitaxially



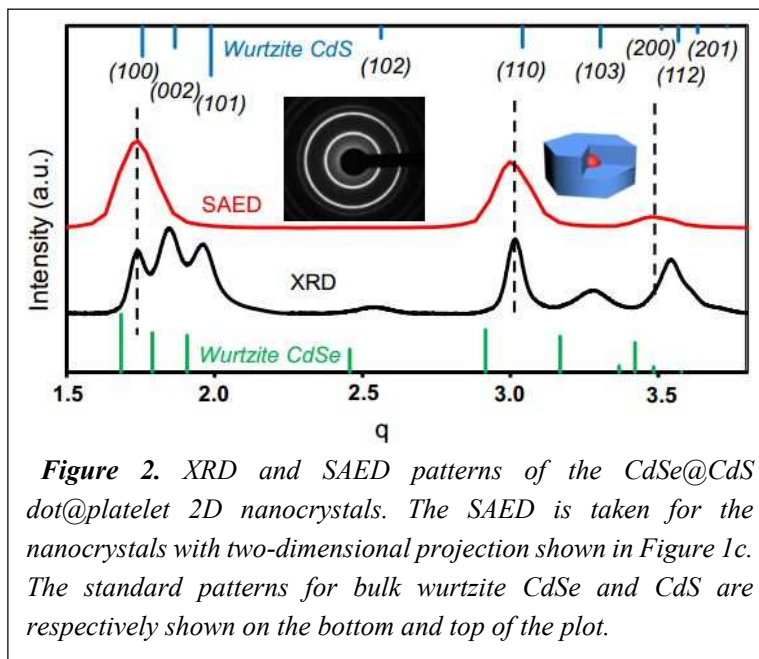
grown onto 3.2 nm wurtzite CdSe cores through the scheme in Figure 1a. Under TEM, two-dimensional projections of nanocrystals would appear as nearly monodisperse either rectangles (Figures 1b) or hexagons (Figure 1c) in different areas. High-resolution TEM reveals that the short edges of a rectangular two-dimensional projection are parallel to the c-axis of wurtzite lattice (Figures 1d and 1e). Conversely, the c-axis of the nanocrystals with hexagonal/spheroidal projections is found to parallel to the electron beam. These high-resolution TEM results are consistent with the disk-shape morphology for monodisperse CdSe@CdS dot@platelet 2D nanocrystals, with the thickness direction as the c-axis of the wurtzite structure. Furthermore, the disk-shape of the core/shell nanocrystals is verified by rotating the nanocrystals under TEM (Figure S1, Supporting Information).

Different from the trapezoidal (or oblate) side view observed in literature, the side view of CdSe@CdS dot@platelet 2D nanocrystals is nearly defect-free rectangular shape with both basal planes being well faceted (Figures 1d and 1e). Elemental distribution of the CdSe@CdS dot@platelet 2D nanocrystals reveals that the 3.2 nm core CdSe nanocrystal is approximately at the center of a 2D nanocrystal (Figures 1g and 1h).

The XRD pattern (Figure 2) of CdSe@CdS dot@platelet 2D nanocrystals is similar to that of bulk wurtzite CdS with slight shift to the low  $q$  direction, which is expected for epitaxial growth of thin yet wide CdS shells (6 nm along the thickness direction and 10.6 nm diagonally cross

the basal plane) onto a small CdSe core (3.2 nm in diameter). Specifically, while the (100), (110), and (200) peaks—ones perpendicular to the  $c$ -axis—are quite close to the standard peaks of bulk wurtzite CdS, the peaks related to the  $c$ -axis ((002), (101), (102), and (103)) are found to be less shifted from the standard peaks of bulk wurtzite CdSe (Table S1, Supporting Information). This means that the wurtzite lattice of the CdSe core nanocrystals are asymmetrically compressed,<sup>52</sup> with significantly more compression along the lateral directions than along the  $c$ -axis.

While high-resolution TEM images are limited to a few selected nanocrystals, electron diffraction can offer



1  
2  
3 information for an ensemble of nanocrystals. When the concentration of CdSe@CdS dot@platelet 2D  
4  
5  
6 nanocrystals is relatively low for deposition onto the TEM substrates, nearly all 2D nanocrystals would orient  
7  
8 themselves with the thickness direction perpendicular to the substrates, similar to the appearance in Figure 1c.  
9  
10  
11 Figure 2 (inset) shows that selected area electron diffraction (SAED) pattern of a large number of nanocrystals  
12  
13 deposited from a low-concentration solution of 2D nanocrystals result in well-defined diffraction rings. To  
14  
15 illustrate orientation of the 2D nanocrystals, the integrated SAED pattern is also plotted with the same axis of  
16  
17 powder X-ray diffraction (XRD) pattern in Figure 2. Different from the XRD pattern of the same sample, the  
18  
19 SAED pattern in Figure 2 only possesses those (hk0) diffraction peaks. This means that 2D nanocrystals in the  
20  
21 area are dominantly oriented with their c-axis parallel to the electron beam, consistent with the shape assignment  
22  
23 based on high-resolution TEM (Figure 1). In comparison, the SAED and XRD patterns resemble each other for  
24  
25 the dot-shaped CdSe/CdS core/shell nanocrystals formed with the Cd to S precursor ratio being higher than one  
26  
27 to one (Figure S2, Supporting Information), which is similar to the products of the conventional SILAR  
28  
29 approach.<sup>21</sup>  
30  
31  
32  
33  
34  
35  
36  
37

38 Below, SAED would be applied as a convenient tool for identification of the disk-shape of the core/shell  
39  
40 nanocrystals. As long as the concentration of nanocrystals in solution is not very high, the disk-shaped  
41  
42 nanocrystals would most likely to lay on the TEM substrates with their thickness direction perpendicular to the  
43  
44 substrates. SAED patterns would thus offer a clear verification of the anisotropic shape of the nanocrystals as  
45  
46 shown in Figure 2.<sup>48</sup>  
47  
48  
49  
50  
51

52 **Effects of the precursor ratio.** A recent study identified that the rate-limiting step in reaction kinetics for  
53  
54 growth of CdSe nanocrystals is the reaction between the activated Se precursors in the solution and surface  
55  
56

1  
2  
3 cadmium sites.<sup>43</sup> This is so because, for this specific reaction, alkanoate ligands provide strong steric barrier  
4  
5 for the reaction sites (Cd atoms coordinated with carboxylates) on surface of the nanocrystals. Such steric effects  
6  
7 caused by strong surface ligands seem to be general in growth of III-V<sup>53</sup> and other II-VI<sup>54</sup> semiconductor  
8  
9 nanocrystals. Such insights help us to outline the main features of the epitaxy scheme for the 2D nanocrystals  
10  
11 in Figure 1a.  
12  
13  
14  
15  
16  
17

18 In the conventional SILAR epitaxial growth,<sup>21</sup> two types of precursors are added into the reaction solution in  
19  
20 an alternating manner to avoid self-nucleation of the cationic and anionic precursors for the shell growth. The  
21  
22 molar ratio between cationic and anionic precursors during the epitaxial growth of CdS (also other types of)  
23  
24 shells were usually kept not smaller than one to one.<sup>21</sup> It has been proven that when elemental S dissolved in  
25  
26 ODE is applied as the sulfur precursor, only ~70% of it would be converted to reactive sulfur source,<sup>55</sup> which  
27  
28 leaves a relatively high concentration of residual cadmium fatty acid salts (Cd(Fa)<sub>2</sub>) as the surface ligands.  
29  
30  
31  
32  
33  
34

35 According to literature, alkanoates can bond onto cadmium chalcogenides in two distinctive forms.<sup>38, 56-58</sup> On  
36  
37 Cd-rich polar surface, such as the Cd-terminated (001) facet for wurtzite CdSe and CdS, negatively-charged  
38  
39 carboxylate groups coordinate strongly with surface cadmium sites and neutralize their positive charges, which  
40  
41 is known as X-type ligands. On non-polar/neutral facets, such as the (100) and (110) lateral facets of wurtzite  
42  
43 CdSe and CdS (see Figure 1f), the ligands should be neutral cadmium alkanoates, whose cadmium ions are  
44  
45 suggested to weakly interact with the surface Se sites and known as Z-type ligands. Though both forms are  
46  
47 associated with fatty acids, the X-type of ligands (negatively-charged alkanoates) bond to the nanocrystals very  
48  
49 strongly but the Z-type of ligands (neutral Cd(Fa)<sub>2</sub>) are found to bond to the nanocrystals weakly.<sup>58-59</sup> As a  
50  
51 result, surface coverage of the X-type of strong ligands should not be significantly dependent on concentration  
52  
53  
54  
55  
56  
57  
58  
59  
60

1  
2  
3 of the residual Cd(Fa)<sub>2</sub> in the epitaxial solution, while surface bonding of the weak Z-type ligands onto the non-  
4  
5  
6 polar side facets would strongly depend on concentration of the Cd(Fa)<sub>2</sub>.  
7  
8  
9

10 Above analysis suggests that, in order to selectively grow epitaxial CdS shells perpendicular to the c-axis of  
11  
12 CdSe dots, it would be necessary to maintain a low concentration of Cd(Fa)<sub>2</sub> in the solution. Mixing two  
13  
14 precursors, instead of addition in an alternating fashion, should allow timely consumption of cadmium  
15  
16 alkanoates to maintain a low instantaneous concentration of cadmium alkanoates in the solution (Figure 1a). An  
17  
18 excess of sulfur precursors in the mixed solution of the precursors should eliminate accumulation of cadmium  
19  
20 alkanoates during the epitaxy. Dropwise addition should further enable a nearly constant yet low concentration  
21  
22 of cadmium carboxylates. In this hypothesized epitaxial scheme, it would be possible to have the non-polar  
23  
24 lateral facets, such as (100) and (110), to be mostly exposed for epitaxy.  
25  
26  
27  
28  
29  
30

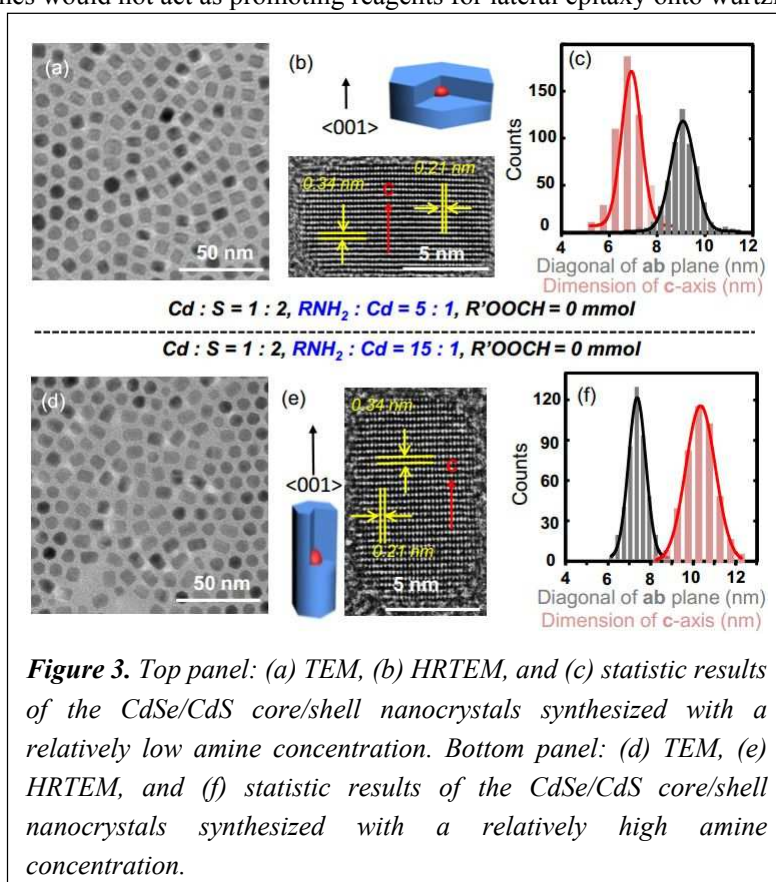
31  
32 Results reveal that, with dropwise addition of the mixed precursors, morphology of the CdSe/CdS core/shell  
33  
34 nanocrystals changes substantially upon varying the Cd to S precursor ratio (Figure S3, Supporting Information).  
35  
36 When the Cd to S precursor ratio in the dropwise-added precursor solution is equal to (or greater than) one, dot-  
37  
38 shaped CdSe/CdS core/shell nanocrystals with poor size distribution are obtained. When the Cd to S precursor  
39  
40 ratio becomes less than one, formation of disk-shaped CdSe/CdS core/shell nanocrystals gradually become  
41  
42 dominating. Under the typical synthetic conditions (see Experimental), nearly monodisperse CdSe@CdS  
43  
44 dot@platelet 2D nanocrystals are reproducibly formed when the Cd to S precursor ratio equals to ~0.5 (Figure  
45  
46 1). If the Cd to S precursor ratio is too low, aggregation of the nanocrystals would become an issue (Figure S3,  
47  
48 Supporting Information). If not mentioned specifically, the Cd to S precursor ratio shall keep 0.5 for formation  
49  
50 of the CdSe@CdS dot@platelet 2D nanocrystals discussed below.  
51  
52  
53  
54  
55  
56

It was reported that fatty amines could remove Z-type ligands on the non-polar facets.<sup>59</sup> However, when epitaxy is performed with the Cd to S precursor ratio greater than one, increasing the concentration of primary amine would not prevent formation of dot-shaped core/shell nanocrystals (Figure S4, Supporting Information). This means that fatty amines could not play the same role of a mixed precursor solution with excess S precursors. Presumably, neutral fatty amines would act as L-type of ligands to passivate the non-polar facets,<sup>57, 60</sup> which is further supported by the additional results in the following sub-section.

**Effects of primary amines.** Figure 3 shows that, without free acid in the epitaxy system, shape of the CdSe/CdS core/shell nanocrystals is strongly affected by the primary amines. However, even with an optimal Cd to S precursor ratio (0.5 to 1), primary amines would not act as promoting reagents for lateral epitaxy onto wurtzite

CdSe core nanocrystals. Instead, it actually increases the relative epitaxial rate along the c-axis (Figure 3).

The top panel of Figure 3 reveals that, for a relatively low concentration of primary amines (5 times of cadmium carboxylates) without free fatty acids, the core/shell nanocrystals is still disk-shaped (Figures 3a and 3b), and



1  
2  
3 thickness direction of the single-crystalline nanocrystals is c-axis of wurtzite structure (Figure 3b and Figure  
4 S5, Supporting Information). However, the lateral/thickness dimension ratio is quite small, only about 1.3  
5  
6 (Figure 3c). In principle, the lateral dimension should be greater than the diameter of the exciton (~10 nm for  
7  
8 CdSe/CdS core/shell nanocrystals) to qualify the core/shell nanocrystals as 2D nanocrystals. Thus, the core/shell  
9  
10 nanocrystals with the average dimensions in Figure 3 (top panel) are quasi-2D nanocrystals. It should be noted  
11  
12 that both basal planes of a quasi-2D nanocrystal in Figure 3 (top panel) are about with the same length and its  
13  
14 side view is rectangular.  
15  
16  
17  
18  
19  
20  
21  
22

23 Figure 3 (bottom panel) shows that, by increasing concentration of the primary amines, shape of the core/shell  
24  
25 nanocrystals actually switches to rod-shape (Figure 3d). As expected, high-resolution TEM measurements  
26  
27 (Figure 3e and Figure S5, Supporting Information) reveal that the long-axis of the core/shell nanocrystals is the  
28  
29 c-axis. XRD patterns in Figure S5 (Supporting Information) further confirm the shape of the nanocrystals  
30  
31 assigned in Figures 3b and 3e.  
32  
33  
34  
35  
36  
37

38 According to the shape assignments described above, the average volume of the disk-shaped (Figure 3c) and  
39  
40 rod-shaped (Figure 3f) CdSe/CdS core/shell nanocrystals is almost the same, indicating concentration of  
41  
42 primary amines does not affect overall epitaxial growth of the CdS shells except switching the preferential  
43  
44 growth direction from lateral axes to c-axis of the wurtzite structure.  
45  
46  
47  
48  
49

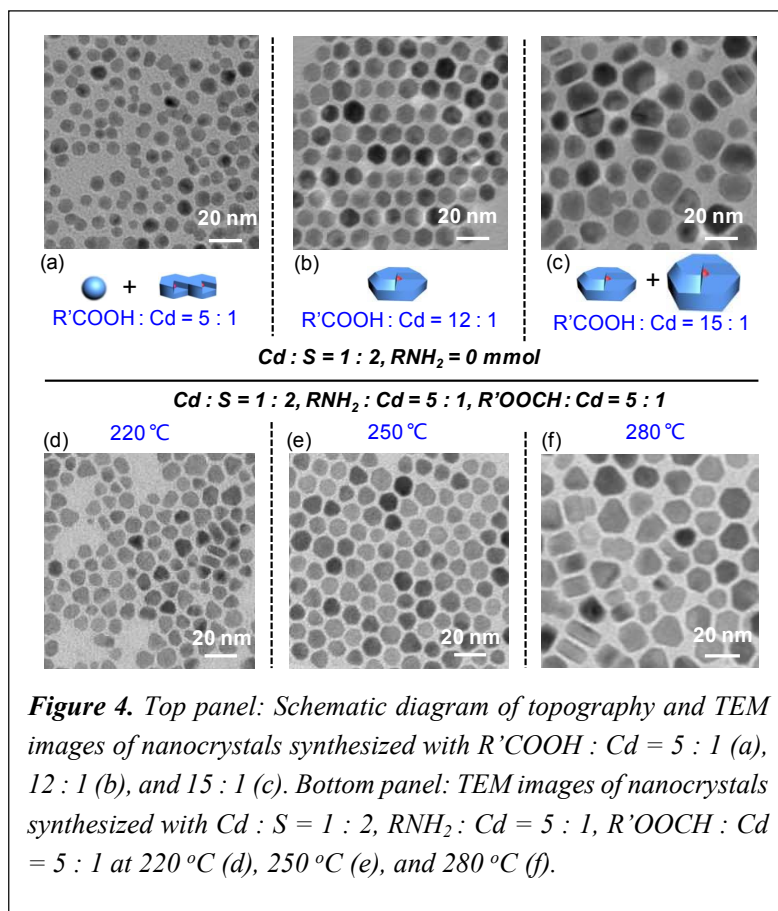
50 As mentioned above, primary amines are known as neutral L-type ligands for the non-polar facets of cadmium  
51  
52 chalcogenide nanocrystals.<sup>38, 44, 57</sup> Their bonding with the surface cadmium sites is weak yet dynamic under  
53  
54 typical growth temperatures.<sup>61</sup> By increasing their concentration in the epitaxial solution, weak and dynamic  
55  
56  
57  
58  
59  
60

1  
2  
3  
4 passivation of the non-polar facets by primary amines would be enhanced. Consequently, this would slow down  
5  
6 the lateral growth relative to the epitaxy along the c-axis and lead to reduced lateral/thickness dimension ratio.  
7  
8 At a very high concentration, passivation of the non-polar facets would become constantly high in the time  
9  
10 domain.<sup>61</sup> As a result, growth long the c-axis—presumably at the Se-terminated [001] facet—becomes  
11  
12 dominating,<sup>37-38</sup> resulting in rod-shaped core/shell nanocrystals.  
13  
14  
15  
16  
17

18 **Effects of fatty acids.** The schematic illustration of the current approach in Figure 1a shows that epitaxial  
19  
20 growth of core/shell 2D nanocrystals relies on a significant excess of the sulfur precursor (elemental S). In  
21  
22 principle, excess S would eventually consume all cadmium carboxylates either in the solution or on the surface  
23  
24 of the nanocrystals. If no other types of ligands—such as fatty amines—in the epitaxial solution, this should  
25  
26 induce precipitation, aggregation, and/or uncontrolled epitaxy. Interestingly, addition of free fatty acids into the  
27  
28 reaction solution solves these problems.  
29  
30  
31  
32  
33  
34

35 Figure 4 (top panel) shows three TEM images for a series of epitaxial reactions without any amines in the  
36  
37 reaction solution and with the molar ratio of cadmium and sulfur precursors being one to two. In place of primary  
38  
39 amines in the precursor solution, free fatty acids in a controlled amount are added into the precursor mixture of  
40  
41 cadmium alkanoates, elemental S, and ODE. As expected, if concentration of free fatty acid is zero, the reaction  
42  
43 solution become turbid/precipitated rapidly and self-nucleation of CdS nanocrystals is inevitable (data not  
44  
45 shown).  
46  
47  
48  
49  
50  
51  
52  
53  
54  
55  
56  
57  
58  
59  
60

When concentration of free fatty acids increases from zero to <5 times of cadmium carboxylates in the precursor solution, appearance of precipitation of the nanocrystals would be gradually delayed and completely eliminated at the concentration of the free fatty acids being ~5 times of cadmium carboxylates. However, oriented-



attachment of the nanocrystals is still evidenced and small nanocrystals—presumably CdS ones formed by self-nucleation of the precursors—are observed (Figures 4a and S6a (Supporting Information)). Evidently, the oriented-attachment occurs at the lateral facets for this specific system (Figure S6a, Supporting Information), which is consistent with low (or none) surface passivation of the non-polar lateral facets as discussed above.

When the molar ratio between free fatty acids and the cadmium precursor reaches ~12 (Figure 4b), nearly monodisperse 2D nanocrystals are formed by the epitaxial growth (see Figure S6b (Supporting Information) for the corresponding SAED). Further increasing the relative concentration of free fatty acids would result in core/shell nanocrystals with a broad size/shape distribution (Figure 4c), likely due to Ostwald ripening caused by high concentration of the free acids.<sup>54</sup>

1  
2  
3  
4 It should be noted that, different from the core/shell nanocrystals synthesized with primary amines, there is a  
5  
6 significant amount of nanocrystals with trapezoidal side view for the reactions with free fatty acids (Figure 4c).  
7  
8 Presumably, this is because, with alkanoates as the only ligands, the side facets would be difficult to maintain  
9  
10 the non-polar facet, i.e. (100) or (110), similar to the case observed by the Chen's group.<sup>42</sup> Primary amines as  
11  
12 L-type neutral ligands would help to maintain these non-polar facets.  
13  
14  
15  
16  
17

18 Results above suggest that free fatty acids added along with the precursors play at least two important roles.  
19  
20 Firstly, a certain amount of free fatty acids is needed to dissolve tiny CdS nanocrystals formed by self-nucleation,  
21  
22 which has been repeatedly observed in synthesis of II-VI semiconductor nanocrystals.<sup>54</sup> Secondly, free fatty  
23  
24 acids provide colloidal stability of the 2D nanocrystals, which is a new role specifically needed for a synthetic  
25  
26 system requiring an excess amount of anionic precursors.  
27  
28  
29  
30  
31  
32

33 It is known that, at elevated temperatures, elemental sulfur would react with ODE to form reactive sulfur species,  
34  
35 such as H<sub>2</sub>S.<sup>55</sup> These activated S species would react with CdSe core (or CdSe/CdS core/shell) nanocrystals in  
36  
37 the solution under the given reaction conditions. On the polar facets (or the basal planes of the 2D nanocrystals),  
38  
39 H<sub>2</sub>S should react with the Cd sites with carboxylate ligands (RCOO-Cd) and result in formation of HS-Cd  
40  
41 surface species and fatty acids.<sup>43, 55, 62</sup> On the non-polar facets (or the neutral lateral facets), H<sub>2</sub>S should simply  
42  
43 adsorb onto the Cd sites.<sup>43, 63</sup> If there is neither sufficient amount of free fatty acids nor excess cadmium  
44  
45 carboxylates in the epitaxy solution, the resulting nanocrystals would precipitate from the solution due to lack  
46  
47 of surface organic ligands. However, when there is a reasonable concentration of free fatty acids in the solution,  
48  
49 fatty acids could react with the newly formed HS-Cd surface species on the polar facets to release gaseous H<sub>2</sub>S.  
50  
51  
52  
53  
54

55 <sup>64</sup> This would efficiently prevent the growth along the thickness direction by converting the polar facets back to  
56  
57

1  
2  
3 the original structure (RCOO-Cd) and thickness before the reaction with H<sub>2</sub>S. Conversely, on the non-polar  
4 facets for lateral growth, there is no chemical reaction between free fatty acids and the surface adsorbed H<sub>2</sub>S.  
5  
6 Thus, fatty acids would not impact the lateral growth needed for formation of the 2D nanocrystals.  
7  
8  
9

10  
11  
12  
13 There is the third role of free fatty acids in the epitaxy system for 2D nanocrystals. By applying cadmium  
14 alkanoates and free fatty acids with sufficiently different chain lengths, colloidal stability of the resulting 2D  
15 nanocrystals would be ensured. Such a system of entropic ligands is especially important for the nanocrystals  
16 with extended dimensions,<sup>65-66</sup> whose colloidal stability in the solution is often an issue with regular ligands.  
17  
18  
19  
20  
21  
22  
23  
24

25 **Effects of epitaxy temperature.** Results above indicate that chemical reactions involved in epitaxial growth of  
26 the CdS shells onto CdSe core nanocrystals using excess anionic precursors are quite rich. Consequently, one  
27 would suspect that reaction temperature should play an important role for formation of monodisperse 2D  
28 nanocrystals. To study effects of epitaxial temperature, it would be a good idea to exclude influence of the  
29 solution composition. Results in the above sub-section reveal that free fatty acids are essential for the epitaxial  
30 growth of the 2D nanocrystals by dropwise addition of a mixed precursor solution with excess anionic  
31 precursors. However, the resulting 2D nanocrystals are sometimes found to appear with trapezoidal side view  
32 (see examples in Figure 4c), which can be converted to the ones with rectangular side view by addition of fatty  
33 amines (see examples in Figure 3). These observations help us to select a specific composition for studying  
34 effects of epitaxy temperature, which includes both free fatty acids and primary amines in a proper concentration  
35 (Figure 4, bottom panel).  
36  
37  
38  
39  
40  
41  
42  
43  
44  
45  
46  
47  
48  
49  
50  
51  
52  
53  
54

55 With the given solution composition and dropwise addition of the mixed precursor solution, epitaxial  
56

1  
2  
3 temperature is found not to affect the disk-shape of the core/shell nanocrystals (Figure 4, bottom panel). At a  
4  
5 relatively low reaction temperature (such as 220 °C), the lateral size distribution of the 2D nanocrystals is quite  
6  
7 broad with some small dots (Figure 4d), presumably due to insufficient dissolution of small CdS nanocrystals  
8  
9 formed by self-nucleation of the shell precursors.<sup>48</sup> In principle, because of existence of fatty amines, reactivity  
10  
11 of free fatty acids with tiny CdS nanocrystals would increase by increasing the temperature. This hypothesis is  
12  
13 consistent with the nanocrystals epitaxially grown at ~250 °C, i.e., nearly monodisperse CdSe@CdS  
14  
15 dot@platelet 2D nanocrystals (Figure 4e). At even high temperatures (such as 280 °C), the lateral size  
16  
17 distribution is also broad and the average size is quite large (Figure 4f), indicating some degree of Ostward  
18  
19 ripening.  
20  
21  
22  
23  
24  
25  
26  
27

28 **Control of lateral and thickness dimensions of 2D nanocrystals.** The systematic studies summarized above  
29  
30 help us to finalize the scheme for synthesis of nearly monodisperse CdSe@CdS dot@nanoplatelet 2D  
31  
32 nanocrystals (Top of Figure 5). In addition to the composition specified for the precursor solution, a small  
33  
34 amount of fatty amines (~20% of that in the precursor solution) are added into the reaction solution with the  
35  
36 CdSe core nanocrystals to further ensure stability of the core nanocrystals.  
37  
38  
39  
40  
41  
42  
43  
44  
45  
46  
47  
48  
49  
50  
51  
52  
53  
54  
55  
56  
57  
58  
59  
60

Figure 5a shows that, upon dropwise addition of the precursor solution, dimension of the two-dimensional projection of the nanocrystals deposited from low-concentration solutions increases steadily and the size distribution remains nearly monodisperse.

By plotting the average area of these two-dimensional projections versus the epitaxy time, one would see a super-linear function in the early stage followed by a straight line  $\sim 40$  minutes after the reaction (Figure S7, Supporting Information). These features are found to be consistent with two-stage epitaxy, i.e., three-dimensional epitaxy in the first 40 minutes and 2D epitaxy in the late stage, given the constant rate for dropwise addition of the precursors.

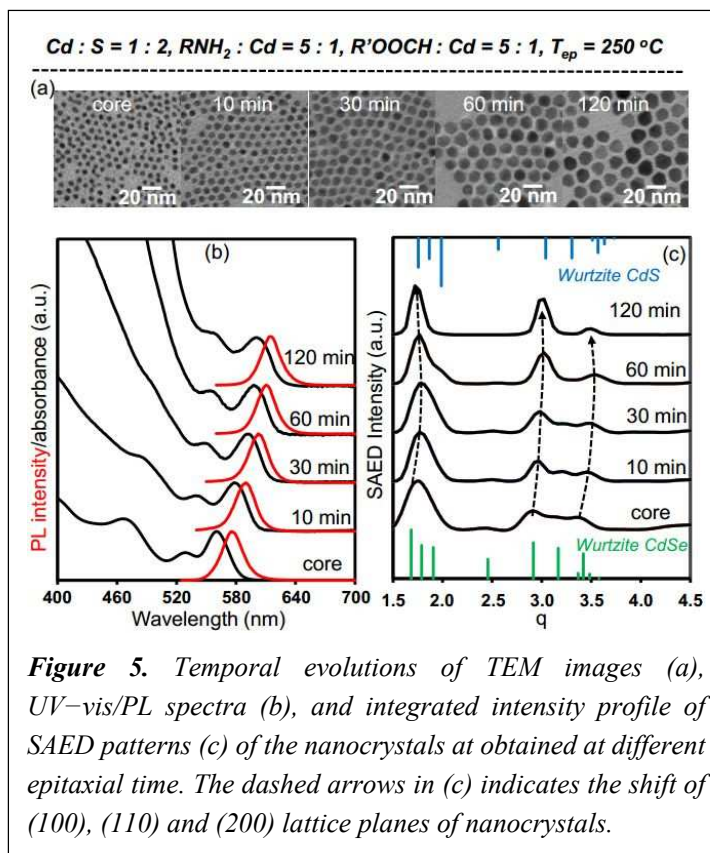


Figure 5b demonstrates that, within  $\sim 120$  minutes of reaction, epitaxial growth of the CdS shells onto CdSe core nanocrystals causes continuous red shift of both UV-Vis absorption and PL spectra due to partial delocalization of photo-generated electron-hole pair (exciton) into the CdS shells.<sup>67</sup> Both UV-Vis and PL spectra of the core/shell nanocrystals retain the sharp features of the core nanocrystals, consistent with the nearly monodisperse size/shape distribution along the lateral directions (Figures 5a and Figure 6) and the thickness direction (Figure 6).

1  
2  
3  
4 It should be mentioned that optical properties of the core/shell nanocrystals at the late stage (>40 min) in Figure  
5  
6 5b are consistent with the shape assignment. For instance, at 120 minutes, the dimension of two-dimensional  
7  
8 projection of the nanocrystals deposited from a low-concentration solution is greater than 10 nm (right picture,  
9  
10 Figure 5a). However, their absorption peak is only at 600 nm, which is blue-shifted in comparison with that  
11  
12 (~604 nm) of spherical CdSe/CdS core/shell nanocrystals with ~8 nm two-dimension projection in Figure S2  
13  
14 (Supporting Information). Figure S8 (Supporting Information) shows that, from 120 minutes to 320 minutes,  
15  
16 both UV-Vis and PL peak show negligible shift while the average lateral dimension of the 2D nanocrystals—  
17  
18 with the same thickness—increases from 10.3 to 16.6 nm. Furthermore, the results in Figure S8 (Supporting  
19  
20 Information) suggest that the growth at the late stage of the optimized epitaxy scheme is not through dissolution  
21  
22 of the existing core/shell CdSe/CdS nanocrystals. The latter case is equivalent to growth of CdSe (or CdSeS)  
23  
24 onto the nanocrystals, which should red-shift the absorption peak significantly.  
25  
26  
27  
28  
29  
30  
31  
32

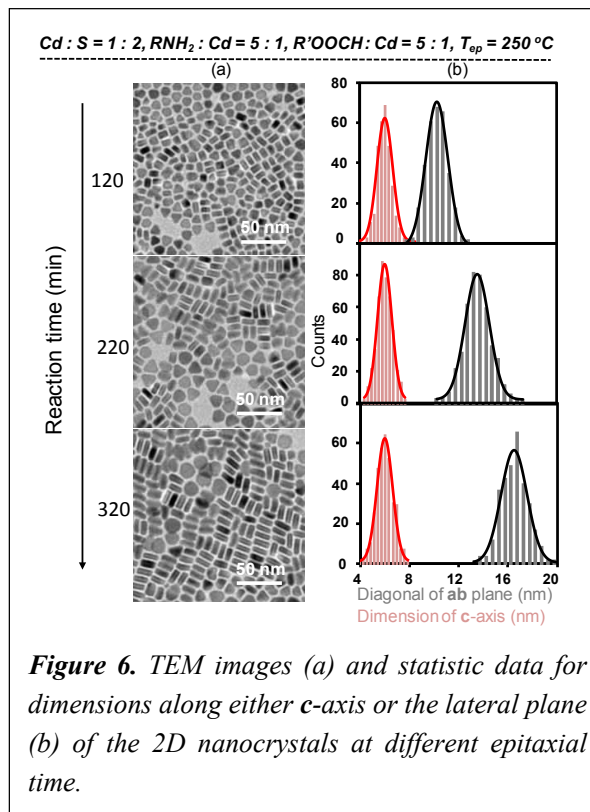
33 For the samples in Figures 5a and 5b, SAED patterns of the nanocrystals deposited from low-concentration  
34  
35 solutions are shown in Figure 5c. As size of the two-dimension projections increases by the epitaxial growth  
36  
37 (Figure 5a), the SAED patterns of the nanocrystals gradually change from random orientation to a specific  
38  
39 orientation, i.e., with the c-axis parallel to the electron beam. The samples beyond 120 minutes of epitaxial  
40  
41 growth possess similar SAED pattern of the sample at 120 minutes (Figure S9, Supporting Information).  
42  
43  
44  
45  
46  
47

48 As mentioned above, when the nanocrystals are deposited onto TEM substrates from the concentrated solutions,  
49  
50 TEM measurements would observe both types of orientations, namely, with the thickness direction either  
51  
52 perpendicular or parallel to the substrate (Figure 6a). The statistic results of more than 300 nanocrystals with a  
53  
54 specific orientation for each sample are shown in Figure 6b. Overall, upon epitaxial growth of the CdS shells  
55  
56  
57  
58  
59  
60

1  
2  
3 onto the CdSe core nanocrystals, the thickness remains the same but the lateral dimension increases steadily  
4  
5  
6 within the timeframe shown in Figure 6. For both  
7  
8 dimensions, their distribution remains narrow, with  
9  
10 the standard deviation being 6-10%.

11  
12  
13  
14  
15 The results in Figure 3 suggest a pathway to control  
16  
17 the thickness of CdSe@CdS dot@platelet 2D  
18  
19 nanocrystals with a given core size. Figure S10  
20  
21 (Supporting Information) illustrates that, by  
22  
23 increasing the amine concentration in the precursor  
24  
25 solution to two times of that shown in Figure 5, one  
26  
27 can increase thickness of the monodisperse 2D  
28  
29 nanocrystals from 6 to 8 nm.  
30  
31  
32  
33  
34  
35  
36  
37

38 **Electronic traps and ensemble optical properties of CdSe@CdS dot@platelet 2D nanocrystals.** Based on  
39  
40 the systematic studies above, a relatively simple and reproducible scheme is developed for epitaxial growth of  
41  
42 CdSe@CdS dot@platelet 2D nanocrystals with tunable shell thickness and lateral dimensions. However, excess  
43  
44 sulfur species on spherical CdSe/CdS core/shell nanocrystals are known as deep hole traps, which greatly  
45  
46 decrease PL quantum yield (QY) of the nanocrystals and complicates PL decay dynamics.<sup>63</sup> Evidently, the  
47  
48 same issue occurs to the 2D nanocrystals. To optimize their PL properties, the as-synthesized 2D nanocrystals  
49  
50 are treated by a sulfur-amine solution and followed by UV radiation (see Experimental for detail). As shown in  
51  
52 Figure 7a, after the surface treatment, PL QY of the 2D nanocrystals increases from ~20% to near unity.  
53  
54  
55  
56  
57  
58  
59  
60



Consistent with their near-unity PL QY, the PL decay dynamics of the 2D nanocrystals after the surface treatment becomes mono-exponential (fitting goodness ( $\chi_R^2$ ) being 1.02) within three orders of magnitude (Figure 7b).

With an optimized concentration, the 2D nanocrystals with mono-exponential PL decay dynamics and unity PL QY are spin-coated onto solid substrates. TEM measurements of a large area of the film (~3000 nanocrystals) reveal that nearly all nanocrystals are oriented themselves with their thickness direction perpendicular to the substrate (Figure S11, Supporting Information). With a fixed direction of the excitation laser (see Experimental),

optical measurements reveal that the 2D nanocrystals in thin films show strongly polarized emission (Figure 7c). Assuming the emission dipole moment of a 2D nanocrystal lies in the lateral plane and perpendicular to the thickness direction, the obtained theoretical pattern matches the experimental results quantitatively (Figure 7c).<sup>68</sup> Both experimental and theoretical results reveal that the maximum polarization factor of the wurtzite CdSe@CdS dot@platelet 2D

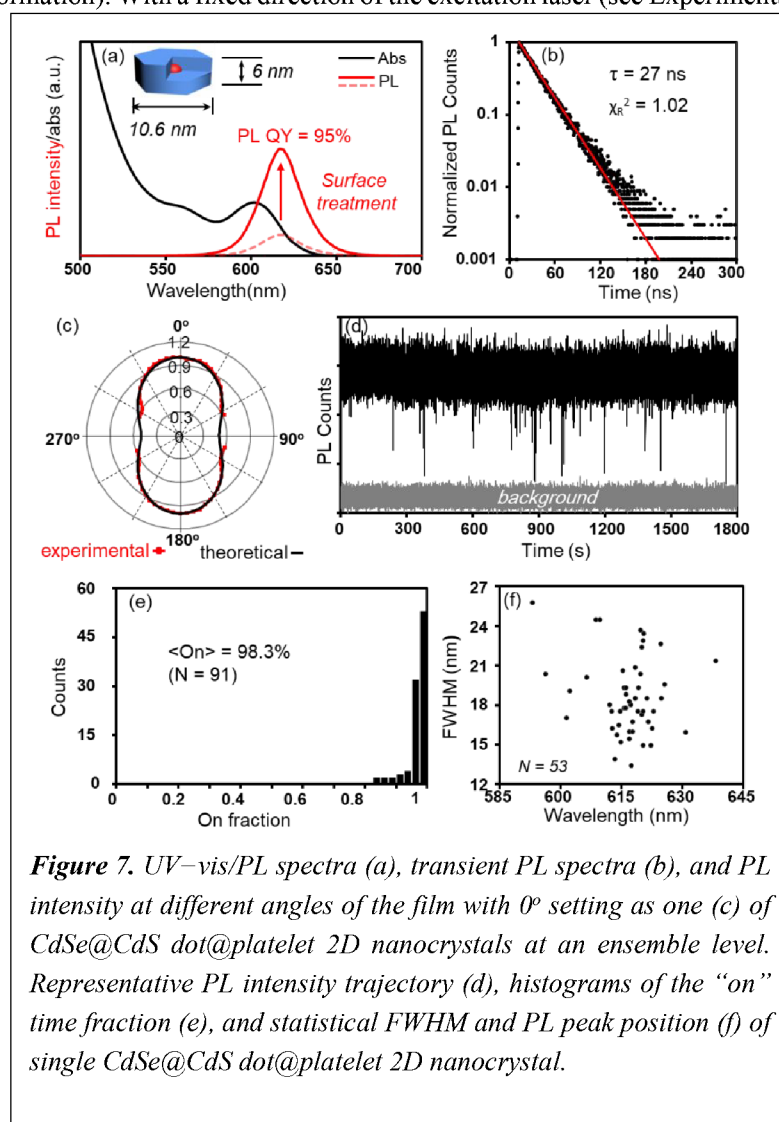


**Figure 7.** UV-vis/PL spectra (a), transient PL spectra (b), and PL intensity at different angles of the film with  $0^\circ$  setting as one (c) of CdSe@CdS dot@platelet 2D nanocrystals at an ensemble level. Representative PL intensity trajectory (d), histograms of the “on” time fraction (e), and statistical FWHM and PL peak position (f) of single CdSe@CdS dot@platelet 2D nanocrystal.

1  
2  
3 nanocrystals is  $\sim 0.5$ , which is comparable with that observed for zinc-blende CdSe 2D nanocrystals with a few  
4  
5  
6 atomic monolayers of Cd and Se atoms.<sup>13, 69</sup>  
7  
8  
9

10  
11 It was reported that, in either UV-Vis absorption or PL excitation (PLE) spectra, splitting of the first exciton  
12  
13 state—the first absorption peak becoming doublet—was observed for wurtzite CdSe@CdS dot@platelet 2D  
14  
15 nanocrystals.<sup>10, 12, 27</sup> This was suggested as a result of the anisotropic compression of CdSe core by the CdS  
16  
17 shells along and perpendicular to the c-axis of the wurtzite lattice.<sup>10, 52</sup> Splitting of the first exciton state by  
18  
19 anisotropic compression was also suggested as the origin of the 2D transition dipole of exciton within the lateral  
20  
21 plane.<sup>10</sup> The lateral/thickness dimension ratio of the 2D nanocrystals reported here is likely the largest and its  
22  
23 monodispersity is outstanding. Thus, if there is a significant splitting of the first exciton state, it should be  
24  
25 readily observed. Quantitatively, for typical wurtzite CdSe@CdS dot@platelet 2D nanocrystals described here,  
26  
27 the splitting of the first exciton state can reach 60-70 meV,<sup>10</sup> which should result in a set of well-resolved  
28  
29 doublet in the sharp UV-Vis and PLE spectra.  
30  
31  
32  
33  
34  
35  
36  
37

38 Though polarized emission can be reproducibly observed (Figure 7c), splitting of the first exciton state in the  
39  
40 UV-Vis absorption spectra is not observed (See Figures 6b and 7a for example). The PLE spectra also don't  
41  
42 show splitting of the first exciton state (Figure S12, Supporting Information). Figure S12 (Supporting  
43  
44 Information) also shows that the first exciton state remains as a singlet for our monodisperse wurtzite  
45  
46 CdSe@CdS dot@platelet 2D nanocrystals with different lateral/thickness ratio and/or different thickness.  
47  
48 Furthermore, both peak width and peak contour of the UV-Vis spectra of dot-shaped CdSe/CdS core/shell  
49  
50 nanocrystals are similar to those of the 2D nanocrystals with the same absorption peak position (Figure S13,  
51  
52 Supporting Information).  
53  
54  
55  
56

1  
2  
3  
4  
5  
6 The results described in the above paragraph have two implications. Firstly, orientation of emission transition  
7  
8 dipole within the lateral plane and splitting of the first exciton state are not directly related to each other.  
9  
10 Secondly, because the lattice compression of the CdSe core by the CdS shells along and perpendicular to c-axis  
11  
12 is found to differ from each other slightly, i.e., 3.7% for [100] direction versus 3.0% for [001] direction (Table  
13  
14 S1, Supporting Information), it might be insufficient to cause significant splitting of the first exciton state.<sup>52</sup>  
15  
16  
17  
18  
19

20 It is interesting to notice that the CdSe dots are located on one side of the wurtzite CdSe/CdS core/shell  
21  
22 nanocrystals reported by the Sargent group, which implies asymmetric compression along the thickness  
23  
24 direction.<sup>12</sup> Possibly, splitting of the first exciton state requires symmetry breaking along the c-axis but  
25  
26 orientation of the emission transition dipole within the lateral plane is associated with the relative localization  
27  
28 of the electron and hole wavefunctions within the lateral plane.  
29  
30  
31  
32  
33  
34

35 **PL of single 2D nanocrystal.** Single-molecular spectroscopy can reveal some special properties of  
36  
37 semiconductor nanocrystals. In 1996, PL intensity of single colloidal semiconductor nanocrystal was observed  
38  
39 to randomly switch between different brightness states under constant excitation—PL blinking—due to photo-  
40  
41 induced ionization and deionization of the nanocrystal.<sup>29</sup> PL blinking causes serious issues for semiconductor  
42  
43 nanocrystals as emitters in most applications.<sup>70-72</sup> After over 20 years of efforts, suppression of PL blinking has  
44  
45 recently made some progress, especially for spherical CdSe/CdS core/shell nanocrystals.<sup>30, 51, 73-75</sup> However, to  
46  
47 our knowledge, there is no report of PL non-blinking for single 2D nanocrystal.  
48  
49  
50  
51  
52  
53  
54

55 PL peak position of single 2D nanocrystal is found to vary somewhat around that of the ensemble PL but the  
56  
57  
58  
59  
60

1  
2  
3  
4 sum PL spectrum of multiple 2D nanocrystals reproduces that of the ensemble PL in the solution (Figure S14,  
5  
6 Supporting Information). PL decay dynamics reveals that the single-nanocrystal PL is purely single-exciton  
7  
8 emission, with the mono-exponential PL decay lifetime comparable with that of the ensemble PL (Figure S14,  
9  
10 Supporting Information). The second-order correlation measurements confirm that the PL measurements for  
11  
12 single-molecular spectroscopy are for single 2D nanocrystal (Figure S14, Supporting Information).  
13  
14  
15  
16  
17

18 Figure 7d illustrates a typical PL intensity trajectory for a CdSe@CdS dot@platelet 2D nanocrystal with 6 nm  
19  
20 in thickness and 10.6 nm for lateral dimension. Though the CdS shells for the core nanocrystal are only ~4  
21  
22 monolayers along the thickness direction, CdSe@CdS dot@platelet 2D nanocrystal is nearly non-blinking under  
23  
24 prolonged excitation (1800 seconds for Figure 7d). Figure 7d shows that the 2D nanocrystal occasionally  
25  
26 switches from the bright state to the dim state, which corresponds to photo-induced ionization—losing the hole  
27  
28 to the surroundings—of the 2D nanocrystal.<sup>29</sup> The probability of photo-induced ionization of the 2D  
29  
30 nanocrystals is only  $\sim 10^{-7}$ , which is about 2 orders of magnitudes lower than the optimal spherical CdSe/CdS  
31  
32 core/shell nanocrystals with similar total volume.<sup>75</sup> Given the relatively thin shells along the thickness direction,  
33  
34 such outstanding resistance to photo-induced ionization is surprising. Figure 7d further demonstrates that each  
35  
36 duration of the dim state is very short, typically within one bin (30 ms), indicating rapid deionization of the  
37  
38 photo-ionized nanocrystal.<sup>75</sup> Statistically, extremely low frequency of photo-induced ionization and short dim-  
39  
40 state duration result in a high “on” time fraction (Figure 7e). At present, we don’t know the reason(s) behind  
41  
42 the outstanding properties in Figures 7d and 7e. We suspect that it should be a result of the well-defined surface  
43  
44 structure of CdSe@CdS dot@platelet 2D nanocrystals, especially the basal planes, and confinement of the holw  
45  
46 wavefunction towards the center along the thickness direction.  
47  
48  
49  
50  
51  
52  
53  
54  
55  
56  
57  
58  
59  
60

1  
2  
3  
4 Figure 7f summarizes the full width at half-maximum (FWHM) of single-nanocrystal PL versus the PL peak  
5  
6 position. Evidently, PL FWHM values of single CdSe@CdS dot@platelet 2D nanocrystals are about the same  
7  
8 as those of spherical CdSe/CdS core/shell nanocrystal,<sup>51, 75-76</sup> and the single-nanocrystal PL spectrum is  
9  
10 symmetric (Figure S14, Supporting Information). Specifically, the statistic PL peak position and FWHM are  
11  
12 with narrow distribution and respectively centralized at 617 nm and 18 nm. Thus, single-nanocrystal  
13  
14 spectroscopy measurements also against existence of splitting of the first exciton state for the current system of  
15  
16 2D nanocrystals. As mentioned above, splitting of the first exciton state would increase energy difference  
17  
18 between the heavy hole and light hole to about 60-70 meV, which is much greater than the thermal energy at  
19  
20 ambient temperatures and should thus significantly reduce the PL FWHM to below thermal energy, at least at  
21  
22 a single-nanocrystal level.<sup>12, 52</sup>  
23  
24  
25  
26  
27  
28  
29

## 30 CONCLUSION

31  
32  
33 In summary, epitaxy of CdS shells onto dot-shaped CdSe core nanocrystals can be well controlled to form size-  
34  
35 and shape-monodisperse CdSe@CdS dot@platelet 2D nanocrystals. For the shape-selective epitaxy, free fatty  
36  
37 acids are surprisingly playing a key role and dropwise addition of a mixed precursor solution with significant  
38  
39 excess of the sulfur precursor is essential. PL properties of the 2D nanocrystals can be boosted to be comparable  
40  
41 with spheroidal CdSe/CdS core/shell nanocrystals, i.e., with near-unity PL quantum yield, mono-exponential  
42  
43 PL decay dynamics, and single-nanocrystal PL non-blinking. Unique PL properties of the 2D nanocrystals are  
44  
45 identified, including polarized PL and extremely low PL blinking probability (about 2 orders of magnitudes  
46  
47 lower than the spheroidal counterparts). Neither splitting of the first excitonic absorption state nor ultra-narrow  
48  
49 PL (~25 meV at room temperature) of single 2D nanocrystal is observed. Insights on synthesis of high-  
50  
51 performance CdSe@CdS dot@platelet 2D nanocrystals offer design principles for realizing other types of 2D  
52  
53  
54  
55  
56  
57  
58  
59  
60

1  
2  
3  
4 nanocrystals. The resulting 2D nanocrystals, including those disclosed here and others to be developed, should  
5  
6 offer a unique set of nanocrystal emitters for various applications. For example, polarized emission from readily  
7  
8 aligned 2D nanocrystals would increase the theoretical limit of external quantum yield of light-emitting-diodes  
9  
10  
11 with typical device structures by ~50%.<sup>77-80</sup>  
12  
13  
14  
15  
16  
17

## 18 EXPERIMENTAL SECTION

19  
20  
21  
22

23 **Chemicals.** Stearic acid (90+%), octanoic acid (HOc, 90%), trioctylphosphine oxide (TOPO,90%), octadecylamine  
24 (90%), tetramethylammonium hydroxide (98%), cadmium oxide (CdO, 99.998%), selenium power (200 mesh,  
25 99.999%), 1-octadecene (ODE, 90%), n-octane (98%+) and oleic acid (HOl, 90%) were purchased from Alfa-Aesar.  
26  
27 Tributylphosphine (TBP) was purchased from Acros. Sulfur powder (S, 99.98%), cadmium formate (Cd(Fo)<sub>2</sub>, 99.9%),  
28 octylamine (99%) and oleylamine (NH<sub>2</sub>Ol, 70%) were purchased from Aldrich. Cadmium acetate dihydrate  
29 (Cd(Ac)<sub>2</sub>·2H<sub>2</sub>O, 98.5%) was purchased from Shanghai Tingxin Reagents. All organic solvents were purchased from  
30 Sinopharm Reagents. All chemicals were used directly without any further purification.  
31  
32  
33  
34  
35  
36

37 **Preparation of the Cadmium Oleate (Cd(Ol)<sub>2</sub>) Precursors.** HOl (20 mmol) and 20 mmol of tetramethylammonium  
38 hydroxide were dissolved in 200 mL of methanol. Cd(Ac)<sub>2</sub>·2H<sub>2</sub>O (10 mmol) dissolved in 50 mL of methanol was  
39 added dropwise to this solution under vigorous stirring. White Cd(Ol)<sub>2</sub> immediately precipitated, and the mixture  
40 was stirred for another 20 min after adding Cd(Ac)<sub>2</sub> solution to ensure the reaction was completed. The precipitates  
41 were washed three times with methanol and dried under vacuum overnight.  
42  
43  
44  
45  
46  
47

48 **Preparation of the Se Precursor.** A 0.1 mol/L TBP–Se solution was made by dissolving 10 mmol of Se powder in  
49 2.36 g of TBP in a glovebox, which was further diluted with 6.85 g of ODE.  
50  
51  
52  
53

54 **Preparation of the Mixed Precursors.** Cd(Ol)<sub>2</sub> (0.2277g, 0.3 mmol) and appropriate amount of S were dissolved in  
55 a mixture of NH<sub>2</sub>Ol, HOl (or HOc), and ODE with a total volume of 3 mL. For synthesis of a typical sample  
56  
57  
58  
59  
60

(nanocrystals with their thickness and diagonal of ab plane as 6 nm, and 10.3 nm, respectively), the mixed precursor was prepared as follows: 0.2277g Cd(OI)<sub>2</sub> (0.3 mmol) and 0.0192g (0.6 mmol) of S were dissolved in a mixture of 1.5 mmol NH<sub>2</sub>Ol, 1.5 mmol HOc, and ODE with a total volume of 3 mL. For studies related to Figures 3 4, and S3-S6 (Supporting Information), the amounts of S, NH<sub>2</sub>Ol, HOI (or HOc), and ODE would be changed accordingly.

**Preparation of S-ODE.** 1 mmol of S powder was added to 10 mL of ODE. Ultrasonic treatment was applied to get a clear solution.

**Synthesis of CdSe Core Nanocrystals.** Synthesis of 3.2 nm spherical wurtzite CdSe QDs (the first excitonic absorption peak at 560 nm) was carried out following a literature method.<sup>21</sup> In a typical synthesis, CdO (0.0256 g, 0.0002 mol) and stearic acid (0.2277 g, 0.0008 mol) were loaded into a 25 mL three-neck flask with 2.5mL of ODE. After stirring and argon bubbling for 10 minutes, the mixture was heated to 270 °C to obtain a colorless solution. The temperature of the mixture was reduced to room temperature, and 0.5g TOPO and 1.5g octadecylamine were added into the flask. After stirring and argon bubbling for 10 minutes, the new mixture was heated to 290 °C. At this temperature, 1mL of 0.1 mol/L TBP-Se solution was quickly injected. The growth temperature was then reduced to 250 °C. When the first absorption peak reached 560 nm, the reaction mixture was allowed to cool to room temperature in air. An extraction procedure was used to purify the nanocrystals from side products and unreacted precursors. The nanocrystals remained in the hexanes/chloroform/ODE layer, and the unreacted precursors and excess amines were extracted into the methanol/acetonitrile layer.

**Synthesis of CdSe@CdS Dot@platelet 2D Nanocrystals.** For growth of the anisotropic shell, a hexane solution containing 150 nmol of CdSe core nanocrystals was loaded into a 25 mL three-neck flask with 3 mL of ODE. After stirring and argon bubbling for 10 minutes at room temperature, the reaction solution was further degassed at 120 °C for 20 min to remove the hexane, water, and oxygen inside the reaction solution. Subsequently, the reaction solution was heated to 250 °C with a heating rate of 18 °C/min under nitrogen flow and magnetic stirring. When the temperature reached 230 °C, the mixed precursor solution was dropwise-added into the reaction solution at a rate of 1.5 mL/hr using a syringe pump. The reaction was monitored by UV-Vis and PL by taking needle-tip amounts of aliquots at different time intervals. The resulting CdSe@CdS Dot@platelet nanocrystals were precipitated by adding acetone from the reaction mixture after cooling to room temperature in air, and then redispersed in toluene. The

1  
2  
3 particles were further purified by precipitation-redispersion for two more rounds using toluene as the solvent and  
4 methanol as the precipitation reagent.  
5  
6  
7

8 **Synthesis of Dot-shaped CdSe/CdS Core/shell Nanocrystals.** Synthesis of dot-shaped core/shell nanocrystals was  
9 similar to that of the dot@platelet ones. The differences were as follows, the Cd : S precursor ratio being 5:4, the  
10 amine concentration being two times higher, and the reaction temperature being 270 °C. When the absorption peak  
11 position was similar to the dot@platelet 2D nanocrystals, the reaction mixture was allowed to cool to room  
12 temperature in air.  
13  
14  
15  
16  
17  
18

19 **Removal of Surface Traps of CdSe@CdS Dot@platelet Nanocrystals.** The surface treatment followed a modified  
20 procedure in literature.<sup>63</sup> A mixture of NH<sub>2</sub>OI (2 mL) and 1 mL of ODE was degassed with argon at 160 °C for 10  
21 minutes. After cooling down the mixture to 110 °C, purified CdSe@CdS Dot@platelet nanocrystals ( $1.0 \times 10^{-7}$  mol)  
22 in ODE was added into the flask. Meanwhile, 2 mL S-ODE (0.1 mol/L) was injected. After heating at 110 °C for 20  
23 minutes, the nanocrystals were precipitated by methanol. This process was repeated until the PL intensity was almost  
24 zero, indicating the 2D nanocrystals were fully treated with sulfur. After the S treatment, 0.2 mL TBP was added at  
25 220 °C. After 5 minutes, the reaction mixture was allowed to cool down to 30 °C, cadmium formate (0.2 mL, 0.1  
26 mol/L in octylamine) was added dropwise into the solution. Subsequently, the sample was irradiated under ultraviolet  
27 light for 20min to fully remove the surface traps.  
28  
29  
30  
31  
32  
33  
34  
35  
36  
37

38 **Sample Preparation for Optical Measurements.** For optical measurements in solution, the nanocrystals were  
39 dispersed in hexane with optical density at the wavelength of 500 nm being 0.1 to 0.3. For studying polarized emission,  
40 the purified nanocrystals in octane were spin-coated onto a clean glass coverslip with a speed of 800 rpm/min. For  
41 single-nanocrystal experiments, nanocrystals were dissolved in a PMMA/toluene (2 wt % PMMA) solution, which  
42 was then spin-casted on a clean glass coverslip.  
43  
44  
45  
46  
47  
48

49 **Measurements and Characterization for Ensemble Nanocrystals.** UV–vis spectra were measured on an Analytik  
50 Jena S600 UV–visible spectrophotometer. PL spectra were taken on an Edinburgh Instruments FLS920 spectrometer.  
51 The absolute PL QY was measured by an Ocean Optics FOIS-1 integrating sphere coupled with a QE65000  
52 spectrometer. Specifically, the nanocrystals were dispersed in toluene to obtain a series of solutions with different  
53  
54  
55  
56  
57  
58  
59  
60

1  
2  
3 concentrations but the same volume (200 uL). For the measurement, each sample was hanged in the integrating  
4 sphere and excited by a 453 nm LED lamp. The photon numbers of excitation and fluorescence were recorded  
5 simultaneously by a spectrometer. Pure toluene was used as the blank sample to obtain the photon number of  
6 excitation light. The number of remiaining photons of the fluorescence was plotted against the remaning photons of  
7 the excitation light for all samples, which was fitted in a linear function with high accuracy and the slope is the  
8 absolute PL QY.  
9  
10  
11  
12  
13  
14  
15

16 PL decay dynamics was recorded on a time correlated single-photon counting (TCSPC) spectrofluorometer (FLS920,  
17 Edinburgh Instrument, UK) with a 405 nm picosecond pulsed laser at a repetition frequency of 0.2 MHz. The peak  
18 photon counts for transient PL were 1000. All optical measurements were performed at room temperature.  
19  
20  
21  
22

23 For polarized emission measurements, luminescence spectrum of the nanocrystals deposited onto a glass slide was  
24 recorded with an optical fiber spectrometer (NOVA-EX, Ideaoptics Instruments) at different angles. The glass slide  
25 was fixed onto a sample holder vertically, and the optical fiber was mounted on a mobile stage and rotated around  
26 the glass slide horizontally. To avoid interference of excitation laser, the laser beam was shined onto the sample with  
27 30° degree from the horizontal rotation cycle of the detector.  
28  
29  
30  
31  
32  
33

34 TEM images and SAED patterns were acquired on a Hitachi 7700 transmission electron microscope at 100 kV, and  
35 the nanocrystals were deposited onto copper grids coated with carbon support film. HRTEM images were obtained  
36 using a JEM 2100F transmission electron microscope operated at 200 kV. Titan ChemiSTEM was used to study the  
37 distribution of elements in the nanocrystals. X-ray diffraction patterns were taken on a Rigaku Ultimate-IV X-ray  
38 diffractometer at 40 kV/30 mA using the Cu K $\alpha$  line ( $\lambda = 1.5418 \text{ \AA}$ ).  
39  
40  
41  
42  
43  
44

45 **Optical Measurements for Single Nanocrystal.** Single-nanocrystal spectroscopy was acquired on a far-field epi-  
46 fluorescence inverted microscopy system (Olympus IX 83) with a 60 $\times$  (NA = 1.49) oil immersion objective. The  
47 emission signal of a nanocrystal was imported into an EMCCD camera (Andor iXon Ultra 897) for imaging. The  
48 fluorescence spectra were recorded with an Andor Kymera 193i spectrometer. The PL intensity trajectory of single  
49 nanocrystal was recorded by an Andor ixon Ultra 897 EMCCD. A CW laser (405 nm, PicoQuant) was used as the  
50 excitation light source. The integration time for each data point was 30 ms. The second-order photon correlation  
51  
52  
53  
54  
55  
56

1  
2  
3 study was performed with a Hanbury Brown and Twiss setup with two avalanche photodiodes. The average photon  
4 number ( $\langle N \rangle$ ) of the excitation was below 0.1 to ensure single-exciton excitation.  
5  
6  
7  
8  
9

## 10 **Associated Content**

### 11 **Supporting Information:**

12  
13 Additional figures. This material is available free of charge via the Internet at <http://pubs.acs.org>.  
14  
15  
16  
17  
18  
19  
20  
21

## 22 **Author Information**

### 23 **Corresponding author**

24  
25  
26  
27 [\\*xpeng@zju.edu.cn](mailto:*xpeng@zju.edu.cn)  
28  
29  
30  
31

### 32 **ORCID**

33  
34  
35 Yonghong Wang: 0000-0002-8257-1952  
36

37 Chaodan Pu: 0000-0001-5028-5516  
38

39 Haiyan Qin: 0000-0003-3731-5236  
40

41 Xiaogang Peng: 0000-0002-5606-8472  
42  
43  
44  
45  
46

### 47 **Author Contributions**

48  
49 † These authors contributed equally to this work.  
50  
51  
52  
53

### 54 **Notes**

The authors declare no competing financial interest.

## Acknowledgements

This work is supported by the National Key Research and Development Program of China (2016YFB0401600), Joint NSFC-ISF Research (Grant 21761142009).

## References:

- (1) Brus, L. E., Electron–electron and electron - hole interactions in small semiconductor crystallites: The size dependence of the lowest excited electronic state. *J. Chem. Phys.* **1984**, *80*, 4403-4409.
- (2) Ithurria, S.; Tessier, M. D.; Mahler, B.; Lobo, R. P.; Dubertret, B.; Efros, A. L., Colloidal nanoplatelets with two-dimensional electronic structure. *Nat. Mater.* **2011**, *10*, 936-41.
- (3) Grim, J. Q.; Christodoulou, S.; Di Stasio, F.; Krahne, R.; Cingolani, R.; Manna, L.; Moreels, I., Continuous-wave biexciton lasing at room temperature using solution-processed quantum wells. *Nat. Nanotech.* **2014**, *9*, 891-895.
- (4) Scott, R.; Heckmann, J.; Prudnikau, A. V.; Antanovich, A.; Mikhailov, A.; Owschimikow, N.; Artemyev, M.; Climente, J. I.; Woggon, U.; Grosse, N. B.; Achtstein, A. W., Directed emission of CdSe nanoplatelets originating from strongly anisotropic 2D electronic structure. *Nat. Nanotech.* **2017**, *12*, 1155-1160.
- (5) Giovanella, U.; Pasini, M.; Lorenzon, M.; Galeotti, F.; Lucchi, C.; Meinardi, F.; Luzzati, S.; Dubertret, B.; Brovelli, S., Efficient solution-processed nanoplatelet-based light-emitting diodes with high operational stability in air. *Nano Lett.* **2018**, *18*, 3441-3448.
- (6) Joo, J.; Son, J. S.; Kwon, S. G.; Yu, J. H.; Hyeon, T., Low-temperature solution-phase synthesis of quantum well structured CdSe nanoribbons. *J. Am. Chem. Soc.* **2006**, *128*, 5632-3.

- 1  
2  
3 (7) Ithurria, S.; Dubertret, B., Quasi 2D colloidal CdSe platelets with thicknesses controlled at the  
4 atomic level. *J. Am. Chem. Soc.* **2008**, *130*, 16504-5.  
5  
6  
7 (8) Li, Z.; Qin, H. Y.; Guzun, D.; Benamara, M.; Salamo, G.; Peng, X. G., Uniform thickness and  
8 colloidal-stable CdS quantum disks with tunable thickness: synthesis and properties. *Nano Res.* **2012**,  
9 *5*, 337-351.  
10  
11  
12  
13 (9) Wang, F.; Wang, Y.; Liu, Y. H.; Morrison, P. J.; Loomis, R. A.; Buhro, W. E., Two-dimensional  
14 semiconductor nanocrystals: properties, templated formation, and magic-size nanocluster  
15 intermediates. *Acc. Chem. Res.* **2015**, *48*, 13-21.  
16  
17  
18  
19 (10) Cassette, E.; Mahler, B.; Guigner, J. M.; Patriarche, G.; Dubertret, B.; Pons, T., Colloidal  
20 CdSe/CdS dot-in-plate nanocrystals with 2D-polarized emission. *ACS Nano* **2012**, *6*, 6741-50.  
21  
22  
23 (11) Bouet, C.; Tessier, M. D.; Ithurria, S.; Mahler, B.; Nadal, B.; Dubertret, B., Flat colloidal  
24 semiconductor nanoplatelets. *Chem. Mater.* **2013**, *25*, 1262-1271.  
25  
26  
27  
28 (12) Fan, F.; Voznyy, O.; Sabatini, R. P.; Bicanic, K. T.; Adachi, M. M.; McBride, J. R.; Reid, K. R.;  
29 Park, Y. S.; Li, X.; Jain, A.; Quintero-Bermudez, R.; Saravanapavanantham, M.; Liu, M.; Korkusinski,  
30 M.; Hawrylak, P.; Klimov, V. I.; Rosenthal, S. J.; Hoogland, S.; Sargent, E. H., Continuous-wave  
31 lasing in colloidal quantum dot solids enabled by facet-selective epitaxy. *Nature* **2017**, *544*, 75-79.  
32  
33  
34 (13) Yoon, D. E.; Kim, W. D.; Kim, D.; Lee, D.; Koh, S.; Bae, W. K.; Lee, D. C., Origin of shape-  
35 dependent fluorescence polarization from CdSe nanoplatelets. *J. Phys. Chem. C* **2017**, *121*, 24837-  
36 24844.  
37  
38  
39 (14) Murray, C. B.; Kagan, C. R.; Bawendi, M. G., Synthesis and characterization of monodisperse  
40 nanocrystals and close-packed nanocrystal assemblies. *Annu. Rev. Mater. Sci.* **2000**, *30*, 545-610.  
41  
42  
43 (15) Peng, X. G., An essay on synthetic chemistry of colloidal nanocrystals. *Nano Res.* **2009**, *2*, 425-  
44 447.  
45  
46  
47 (16) Yang, J.; Son, J. S.; Yu, J. H.; Joo, J.; Hyeon, T., Advances in the colloidal synthesis of two-  
48 dimensional semiconductor nanoribbons. *Chem. Mater.* **2013**, *25*, 1190-1198.  
49  
50  
51  
52  
53  
54  
55  
56  
57  
58  
59  
60

- 1  
2  
3 (17)Nasilowski, M.; Mahler, B.; Lhuillier, E.; Ithurria, S.; Dubertret, B., Two-dimensional colloidal  
4 nanocrystals. *Chem. Rev.* **2016**, *116*, 10934-82.  
5  
6  
7 (18)Peng, X.; Manna, L.; Yang, W.; Wickham, J.; Scher, E.; Kadavanich, A.; Alivisatos, A. P., Shape  
8 control of CdSe nanocrystals. *Nature* **2000**, *404*, 59-61.  
9  
10  
11 (19)Sitt, A.; Hadar, I.; Banin, U., Band-gap engineering, optoelectronic properties and applications of  
12 colloidal heterostructured semiconductor nanorods. *Nano Today* **2013**, *8*, 494-513.  
13  
14  
15 (20)Murray, C. B.; Norris, D. J.; Bawendi, M. G., Synthesis and characterization of nearly  
16 monodisperse CdE (E = sulfur, selenium, tellurium) semiconductor nanocrystallites. *J. Am. Chem. Soc.*  
17 **1993**, *115*, 8706-8715.  
18  
19  
20 (21)Li, J. J.; Wang, Y. A.; Guo, W.; Keay, J. C.; Mishima, T. D.; Johnson, M. B.; Peng, X., Large-  
21 scale synthesis of nearly monodisperse CdSe/CdS core/shell nanocrystals using air-stable reagents via  
22 successive ion layer adsorption and reaction. *J. Am. Chem. Soc.* **2003**, *125*, 12567-75.  
23  
24  
25 (22)Christodoulou, S.; Climente, J. I.; Planelles, J.; Brescia, R.; Prato, M.; Martin-Garcia, B.; Khan,  
26 A. H.; Moreels, I., Chloride-induced thickness control in CdSe nanoplatelets. *Nano Lett.* **2018**, *18*,  
27 6248-6254.  
28  
29  
30 (23)Cho, W.; Kim, S.; Coropceanu, I.; Srivastava, V.; Diroll, B. T.; Hazarika, A.; Fedin, I.; Galli, G.;  
31 Schaller, R. D.; Talapin, D. V., Direct synthesis of six-monolayer (1.9 nm) thick zinc-blende CdSe  
32 nanoplatelets emitting at 585 nm. *Chem. Mater.* **2018**, *30*, 6957-6960.  
33  
34  
35 (24)Mahler, B.; Nadal, B.; Bouet, C.; Patriarche, G.; Dubertret, B., Core/shell colloidal semiconductor  
36 nanoplatelets. *J. Am. Chem. Soc.* **2012**, *134*, 18591-8.  
37  
38  
39 (25)Ithurria, S.; Talapin, D. V., Colloidal atomic layer deposition (c-ALD) using self-limiting  
40 reactions at nanocrystal surface coupled to phase transfer between polar and nonpolar media. *J. Am.*  
41 *Chem. Soc.* **2012**, *134*, 18585-90.  
42  
43  
44 (26)Rossinelli, A. A.; Riedinger, A.; Marques-Gallego, P.; Knusel, P. N.; Antolinez, F. V.; Norris, D.  
45 J., High-temperature growth of thick-shell CdSe/CdS core/shell nanoplatelets. *Chem. Commun. (Camb)*  
46  
47  
48  
49  
50  
51  
52  
53  
54  
55  
56  
57  
58  
59  
60

1  
2  
3 **2017**, *53*, 9938-9941.

4  
5 (27) Chauhan, H.; Kumar, Y.; Deka, S., New synthesis of two-dimensional CdSe/CdS core@shell dot-  
6 in-hexagonal platelet nanoheterostructures with interesting optical properties. *Nanoscale* **2014**, *6*,  
7 10347-54.

8  
9  
10  
11 (28) Pu, C.; Qin, H.; Gao, Y.; Zhou, J.; Wang, P.; Peng, X., Synthetic control of exciton behavior in  
12 colloidal quantum dots. *J. Am. Chem. Soc.* **2017**, *139*, 3302-3311.

13  
14  
15 (29) Nirmal, M.; Dabbousi, B. O.; Bawendi, M. G.; Macklin, J. J.; Trautman, J. K.; Harris, T. D.; Brus,  
16 L. E., Fluorescence intermittency in single cadmium selenide nanocrystals. *Nature* **1996**, *383*, 802-  
17 804.

18  
19  
20  
21 (30) Galland, C.; Ghosh, Y.; Steinbruck, A.; Sykora, M.; Hollingsworth, J. A.; Klimov, V. I.; Htoon,  
22 H., Two types of luminescence blinking revealed by spectroelectrochemistry of single quantum dots.  
23  
24  
25  
26 *Nature* **2011**, *479*, 203-7.

27  
28 (31) Galland, C.; Ghosh, Y.; Steinbruck, A.; Hollingsworth, J. A.; Htoon, H.; Klimov, V. I., Lifetime  
29 blinking in nonblinking nanocrystal quantum dots. *Nat. Commun.* **2012**, *3*, 908.

30  
31  
32 (32) Tessier, M. D.; Mahler, B.; Nadal, B.; Heuclin, H.; Pedetti, S.; Dubertret, B., Spectroscopy of  
33 colloidal semiconductor core/shell nanoplatelets with high quantum yield. *Nano Lett.* **2013**, *13*, 3321-8.

34  
35 (33) Son, J. S.; Park, K.; Kwon, S. G.; Yang, J.; Choi, M. K.; Kim, J.; Yu, J. H.; Joo, J.; Hyeon, T.,  
36 Dimension-controlled synthesis of CdS nanocrystals: from 0D quantum dots to 2D nanoplates. *Small*  
37  
38  
39  
40  
41 **2012**, *8*, 2394-402.

42  
43 (34) Lhuillier, E.; Pedetti, S.; Ithurria, S.; Nadal, B.; Heuclin, H.; Dubertret, B., Two-dimensional  
44 colloidal metal chalcogenides semiconductors: synthesis, spectroscopy, and applications. *Acc. Chem.*  
45  
46  
47  
48  
49 *Res.* **2015**, *48*, 22-30.

50  
51 (35) Kormilina, T. K.; Cherevko, S. A.; Fedorov, A. V.; Baranov, A. V., Cadmium chalcogenide  
52 nano-heteroplatelets: creating advanced nanostructured materials by shell growth, substitution, and  
53 attachment. *Small* **2017**, *13*, 1702300.

- 1  
2  
3 (36)Shiang, J. J.; Kadavanich, A. V.; Grubbs, R. K.; Alivisatos, A. P., Symmetry of annealed wurtzite  
4 CdSe nanocrystals: assignment to the C<sub>3v</sub> point group. *J. Phys. Chem.* **1995**, *99*, 17417-17422.  
5  
6 (37)Peng, Z. A.; Peng, X., Nearly monodisperse and shape-controlled CdSe nanocrystals via  
7 alternative routes: nucleation and growth. *J. Am. Chem. Soc.* **2002**, *124*, 3343-53.  
8  
9 (38)Manna, L.; Wang, L. W.; Cingolani, R.; Alivisatos, A. P., First-principles modeling of  
10 unpassivated and surfactant-passivated bulk facets of wurtzite CdSe: a model system for studying the  
11 anisotropic growth of CdSe nanocrystals. *J. Phys. Chem. B* **2005**, *109*, 6183-92.  
12  
13 (39)Son, J. S.; Wen, X. D.; Joo, J.; Chae, J.; Baek, S. I.; Park, K.; Kim, J. H.; An, K.; Yu, J. H.; Kwon,  
14 S. G.; Choi, S. H.; Wang, Z.; Kim, Y. W.; Kuk, Y.; Hoffmann, R.; Hyeon, T., Large-scale soft colloidal  
15 template synthesis of 1.4 nm thick CdSe nanosheets. *Angew. Chem., Int. Ed.* **2009**, *48*, 6861-4.  
16  
17 (40)Liu, Y. H.; Wang, F.; Wang, Y.; Gibbons, P. C.; Buhro, W. E., Lamellar assembly of cadmium  
18 selenide nanoclusters into quantum belts. *J. Am. Chem. Soc.* **2011**, *133*, 17005-13.  
19  
20 (41)Rice, K. P.; Saunders, A. E.; Stoykovich, M. P., Seed-mediated growth of shape-controlled  
21 wurtzite CdSe nanocrystals: platelets, cubes, and rods. *J. Am. Chem. Soc.* **2013**, *135*, 6669-76.  
22  
23 (42)Tan, R.; Yuan, Y.; Nagaoka, Y.; Eggert, D.; Wang, X.; Thota, S.; Guo, P.; Yang, H.; Zhao, J.;  
24 Chen, O., Monodisperse hexagonal pyramidal and bipyramidal wurtzite CdSe-CdS core-shell  
25 nanocrystals. *Chem. Mater.* **2017**, *29*, 4097-4108.  
26  
27 (43)Lai, R.; Pu, C.; Peng, X., On-surface reactions in the growth of high-quality CdSe nanocrystals in  
28 nonpolar solutions. *J. Am. Chem. Soc.* **2018**, *140*, 9174-9183.  
29  
30 (44)Talopin, D. V.; Koeppe, R.; Gotzinger, S.; Kornowski, A.; Lupton, J. M.; Rogach, A. L.; Benson,  
31 O.; Feldmann, J.; Weller, H., Highly emissive colloidal CdSe/CdS heterostructures of mixed  
32 dimensionality. *Nano Lett.* **2003**, *3*, 1677-1681.  
33  
34 (45)Carbone, L.; Nobile, C.; De Giorgi, M.; Sala, F. D.; Morello, G.; Pompa, P.; Hytch, M.; Snoeck,  
35 E.; Fiore, A.; Franchini, I. R.; Nadasan, M.; Silvestre, A. F.; Chiodo, L.; Kudera, S.; Cingolani, R.;  
36 Krahne, R.; Manna, L., Synthesis and micrometer-scale assembly of colloidal CdSe/CdS nanorods  
37  
38  
39  
40  
41  
42  
43  
44  
45  
46  
47  
48  
49  
50  
51  
52  
53  
54  
55  
56  
57  
58  
59  
60

1  
2  
3 prepared by a seeded growth approach. *Nano Lett.* **2007**, *7*, 2942-50.

4  
5 (46) Talapin, D. V.; Nelson, J. H.; Shevchenko, E. V.; Aloni, S.; Sadtler, B.; Alivisatos, A. P., Seeded  
6  
7 growth of highly luminescent CdSe/CdS nanoheterostructures with rod and tetrapod morphologies.

8  
9 *Nano Lett.* **2007**, *7*, 2951-9.

10  
11 (47) Rempel, J. Y.; Trout, B. L.; Bawendi, M. G.; Jensen, K. F., Density functional theory study of  
12  
13 ligand binding on CdSe (0001), (0001), and (1120) single crystal relaxed and reconstructed surfaces:  
14  
15 implications for nanocrystalline growth. *J. Phys. Chem. B* **2006**, *110*, 18007-16.

16  
17 (48) Zhou, J.; Pu, C.; Jiao, T.; Hou, X.; Peng, X., A two-step synthetic strategy toward monodisperse  
18  
19 colloidal CdSe and CdSe/CdS core/shell nanocrystals. *J. Am. Chem. Soc.* **2016**, *138*, 6475-83.

20  
21 (49) Evans, C. M.; Evans, M. E.; Krauss, T. D., Mysteries of TOP-Se revealed: insights into quantum  
22  
23 dot nucleation. *J. Am. Chem. Soc.* **2010**, *132*, 10973-5.

24  
25 (50) Ruberu, T. P.; Albright, H. R.; Callis, B.; Ward, B.; Cisneros, J.; Fan, H. J.; Vela, J., Molecular  
26  
27 control of the nanoscale: effect of phosphine-chalcogenide reactivity on CdS-CdSe nanocrystal  
28  
29 composition and morphology. *ACS Nano* **2012**, *6*, 5348-59.

30  
31 (51) Chen, O.; Zhao, J.; Chauhan, V. P.; Cui, J.; Wong, C.; Harris, D. K.; Wei, H.; Han, H.-S.;  
32  
33 Fukumura, D.; Jain, R. K.; Bawendi, M. G., Compact high-quality CdSe-CdS core-shell nanocrystals  
34  
35 with narrow emission linewidths and suppressed blinking. *Nat. Mater.* **2013**, *12*, 445-451.

36  
37 (52) Park, Y. S.; Lim, J.; Klimov, V. I., Asymmetrically strained quantum dots with non-fluctuating  
38  
39 single-dot emission spectra and subthermal room-temperature linewidths. *Nat. Mater.* **2019**, *18*, 249-  
40  
41 255.

42  
43 (53) Li, Y.; Pu, C. D.; Peng, X. G., Surface activation of colloidal indium phosphide nanocrystals.  
44  
45 *Nano Res.* **2017**, *10*, 941-958.

46  
47 (54) Li, J.; Wang, H.; Lin, L.; Fang, Q.; Peng, X., Quantitative identification of basic growth channels  
48  
49 for formation of monodisperse nanocrystals. *J. Am. Chem. Soc.* **2018**, *140*, 5474-5484.

50  
51 (55) Li, Z.; Ji, Y.; Xie, R.; Grisham, S. Y.; Peng, X., Correlation of CdS nanocrystal formation with  
52  
53

1  
2  
3 elemental sulfur activation and its implication in synthetic development. *J. Am. Chem. Soc.* **2011**, *133*,  
4 17248-56.

5  
6  
7 (56)Fritzinger, B.; Capek, R. K.; Lambert, K.; Martins, J. C.; Hens, Z., Utilizing self-exchange to  
8 address the binding of carboxylic acid ligands to CdSe quantum dots. *J. Am. Chem. Soc.* **2010**, *132*,  
9 10195-201.

10  
11  
12 (57)Anderson, N. C.; Hendricks, M. P.; Choi, J. J.; Owen, J. S., Ligand exchange and the stoichiometry  
13 of metal chalcogenide nanocrystals: spectroscopic observation of facile metal-carboxylate  
14 displacement and binding. *J. Am. Chem. Soc.* **2013**, *135*, 18536-48.

15  
16  
17 (58)Owen, J., Nanocrystal structure. The coordination chemistry of nanocrystal surfaces. *Science* **2015**,  
18 *347*, 615-6.

19  
20  
21 (59)Singh, S.; Tomar, R.; Ten Brinck, S.; De Roo, J.; Geiregat, P.; Martins, J. C.; Infante, I.; Hens, Z.,  
22 Colloidal CdSe nanoplatelets, a model for surface chemistry/optoelectronic property relations in  
23 semiconductor nanocrystals. *J. Am. Chem. Soc.* **2018**, *140*, 13292-13300.

24  
25  
26 (60)Jia, G.; Banin, U., A general strategy for synthesizing colloidal semiconductor zinc chalcogenide  
27 quantum rods. *J. Am. Chem. Soc.* **2014**, *136*, 11121-7.

28  
29  
30 (61)Pradhan, N.; Reifsnyder, D.; Xie, R.; Aldana, J.; Peng, X., Surface ligand dynamics in growth of  
31 nanocrystals. *J. Am. Chem. Soc.* **2007**, *129*, 9500-9.

32  
33  
34 (62)Nag, A.; Kovalenko, M. V.; Lee, J. S.; Liu, W.; Spokoyny, B.; Talapin, D. V., Metal-free inorganic  
35 ligands for colloidal nanocrystals: S<sup>2-</sup>, HS<sup>-</sup>, Se<sup>2-</sup>, HSe<sup>-</sup>, Te<sup>2-</sup>, HTe<sup>-</sup>, TeS<sub>3</sub>(<sup>2-</sup>), OH<sup>-</sup>, and NH<sub>2</sub><sup>-</sup> as  
36 surface ligands. *J. Am. Chem. Soc.* **2011**, *133*, 10612-20.

37  
38  
39 (63)Pu, C.; Peng, X., To battle surface traps on CdSe/CdS core/shell nanocrystals: shell isolation  
40 versus surface treatment. *J. Am. Chem. Soc.* **2016**, *138*, 8134-42.

41  
42  
43 (64)Zhang, H.; Hu, B.; Sun, L.; Hovden, R.; Wise, F. W.; Muller, D. A.; Robinson, R. D., Surfactant  
44 ligand removal and rational fabrication of inorganically connected quantum dots. *Nano Lett.* **2011**, *11*,  
45 5356-61.

- 1  
2  
3 (65) Ghosh, Y.; Mangum, B. D.; Casson, J. L.; Williams, D. J.; Htoon, H.; Hollingsworth, J. A., New  
4 insights into the complexities of shell growth and the strong influence of particle volume in  
5 nonblinking "giant" core/shell nanocrystal quantum dots. *J. Am. Chem. Soc.* **2012**, *134*, 9634-43.  
6  
7  
8  
9 (66) Niu, Y.; Pu, C. D.; Lai, R. C.; Meng, R. Y.; Lin, W. Z.; Qin, H. Y.; Peng, X. G., One-pot/three-  
10 step synthesis of zinc-blende CdSe/CdS core/shell nanocrystals with thick shells. *Nano Res.* **2017**, *10*,  
11 1149-1162.  
12  
13  
14  
15 (67) Laheld, U. E.; Pedersen, F. B.; Hemmer, P. C., Excitons in type-II quantum dots: Finite offsets.  
16 *Phys. Rev. B: Condens. Matter* **1995**, *52*, 2697-2703.  
17  
18  
19 (68) Brokmann, X.; Coolen, L.; Hermier, J. P.; Dahan, M., Emission properties of single CdSe/ZnS  
20 quantum dots close to a dielectric interface. *Chem. Phys.* **2005**, *318*, 91-98.  
21  
22  
23 (69) Cunningham, P. D.; Souza, J. B., Jr.; Fedin, I.; She, C.; Lee, B.; Talapin, D. V., Assessment of  
24 anisotropic semiconductor nanorod and nanoplatelet heterostructures with polarized emission for  
25 liquid crystal display technology. *ACS Nano* **2016**, *10*, 5769-81.  
26  
27  
28  
29 (70) Marchuk, K.; Guo, Y.; Sun, W.; Vela, J.; Fang, N., High-precision tracking with non-blinking  
30 quantum dots resolves nanoscale vertical displacement. *J. Am. Chem. Soc.* **2012**, *134*, 6108-11.  
31  
32  
33  
34 (71) Keller, A. M.; Ghosh, Y.; DeVore, M. S.; Phipps, M. E.; Stewart, M. H.; Wilson, B. S.; Lidke, D.  
35 S.; Hollingsworth, J. A.; Werner, J. H., 3-Dimensional tracking of non-blinking 'giant' quantum dots  
36 in live cells. *Adv. Funct. Mater.* **2014**, *24*, 4796-4803.  
37  
38  
39  
40 (72) Lim, J.; Park, Y. S.; Wu, K.; Yun, H. J.; Klimov, V. I., Droop-free colloidal quantum dot light-  
41 emitting diodes. *Nano Lett.* **2018**, *18*, 6645-6653.  
42  
43  
44  
45 (73) Chen, Y.; Vela, J.; Htoon, H.; Casson, J. L.; Werder, D. J.; Bussian, D. A.; Klimov, V. I.;  
46 Hollingsworth, J. A., "Giant" multishell CdSe nanocrystal quantum dots with suppressed blinking. *J.*  
47 *Am. Chem. Soc.* **2008**, *130*, 5026-7.  
48  
49  
50  
51 (74) Mahler, B.; Spinicelli, P.; Buil, S.; Quelin, X.; Hermier, J. P.; Dubertret, B., Towards non-blinking  
52 colloidal quantum dots. *Nat. Mater.* **2008**, *7*, 659-64.  
53  
54  
55  
56

(75) Meng, R.; Qin, H.; Niu, Y.; Fang, W.; Yang, S.; Lin, X.; Cao, H.; Ma, J.; Lin, W.; Tong, L.; Peng, X., Charging and discharging channels in photoluminescence intermittency of single colloidal CdSe/CdS core/shell quantum dot. *J. Phys. Chem. Lett.* **2016**, *7*, 5176-5182.

(76) Zhou, J.; Zhu, M.; Meng, R.; Qin, H.; Peng, X., Ideal CdSe/CdS core/shell nanocrystals enabled by entropic ligands and their core size-, shell thickness-, and ligand-dependent photoluminescence properties. *J. Am. Chem. Soc.* **2017**, *139*, 16556-16567.

(77) Kim, S. Y.; Jeong, W. I.; Mayr, C.; Park, Y. S.; Kim, K. H.; Lee, J. H.; Moon, C. K.; Brutting, W.; Kim, J. J., Organic light-emitting diodes with 30% external quantum efficiency based on a horizontally oriented emitter. *Adv. Funct. Mater.* **2013**, *23*, 3896-3900.

(78) Brutting, W.; Frischeisen, J.; Schmidt, T. D.; Scholz, B. J.; Mayr, C., Device efficiency of organic light-emitting diodes: Progress by improved light outcoupling. *Phys. Status Solidi A* **2013**, *210*, 44-65.

(79) Tuong Ly, K.; Chen-Cheng, R.-W.; Lin, H.-W.; Shiau, Y.-J.; Liu, S.-H.; Chou, P.-T.; Tsao, C.-S.; Huang, Y.-C.; Chi, Y., Near-infrared organic light-emitting diodes with very high external quantum efficiency and radiance. *Nat. Photonics* **2016**, *11*, 63-68.

(80) Gao, Y.; Weidman, M. C.; Tisdale, W. A., CdSe nanoplatelet films with controlled orientation of their transition dipole moment. *Nano Lett.* **2017**, *17*, 3837-3843.

---

## Table of Contents:

